AD627465

Technical Report 399

J. Ruze
F. I. Sheftman
D. A. Cahlander

Radar Ground-Clutter Shields

19 August 1965

Lincoln Laboratory

MASSACHUSETTS INSTITUTE OF TECHNOLOGY

LINCOLN LABORATORY

RADAR GROUND-CLUTTER SHIELDS

J. RUZE

Division 3

F. I. SHEFTMAN

Group 46

D. A. CAHLANDER

Group 42

TECHNICAL REPORT 399

19 AUGUST 1965

LEXINGTON MASSACHUSETTS

BLANK PAGE

ABSTRACT

Metal shields (or fences) are useful in reducing the ground clutter received by a radar. The design of a clutter shield for an L-band radar employing a 60-ft parabolic reflector with Cassegrainian geometry is verified by scale-model measurements at K_a-band. It is shown that a 100-ft fence, at a distance 500 ft from the radar, will give a nominal one-way clutter reduction of 20 db. Tracking is expected to be virtually unaffected down to about 7.8° in elevation, but the low limit on useful performance is about 4.8°. More than 10-db additional clutter reduction is achieved by cutting rectangular slots in the top edge of the fence. However, these and other periodic structures are subject to "resonances" related to grating lobes. This phenomenon is investigated experimentally on the scale model and explained by a mathematical analysis utilizing the principle of stationary phase. A proposed nonperiodic edge treatment is expected to be free of this troublesome effect.

Accepted for the Air Force
Franklin C. Hudson
Chief, Lincoln Laboratory Office

TABLE OF CONTENTS

GLOSSARY

a	serration width (ft)
b	serration length
D(w)	field diffraction function
d	distance of fence from radar (ft)
E	electromagnetic field
e	Naperian base
f(w), g(w)	auxiliary functions
g	height of observation point behind fence (ft)
h	height of clutter fence (ft)
i	angle of incidence
j	$\sqrt{-1}$
K	temperature (°K)
k	phase constant ($2\pi/\lambda$)
L	distance of fence edge from P
m, n	integers
P	power (watts); a point of observation behind fence
r	distance identical to L
S	one-half of fence length (ft)
w	variable used in diffraction function and Fresnel integrals
x	distance along fence as measured from its center
y	vertical distance below fence edge (ft)
α	signal arrival angle
γ	angle below top of fence in shadow region
δ	lateral displacement of observation point P with respect to fence center
λ	wavelength (ft)
Θ	grating lobe angle; angle of resonance
$\varphi(x)$	serration phase function
Δ	incremental change

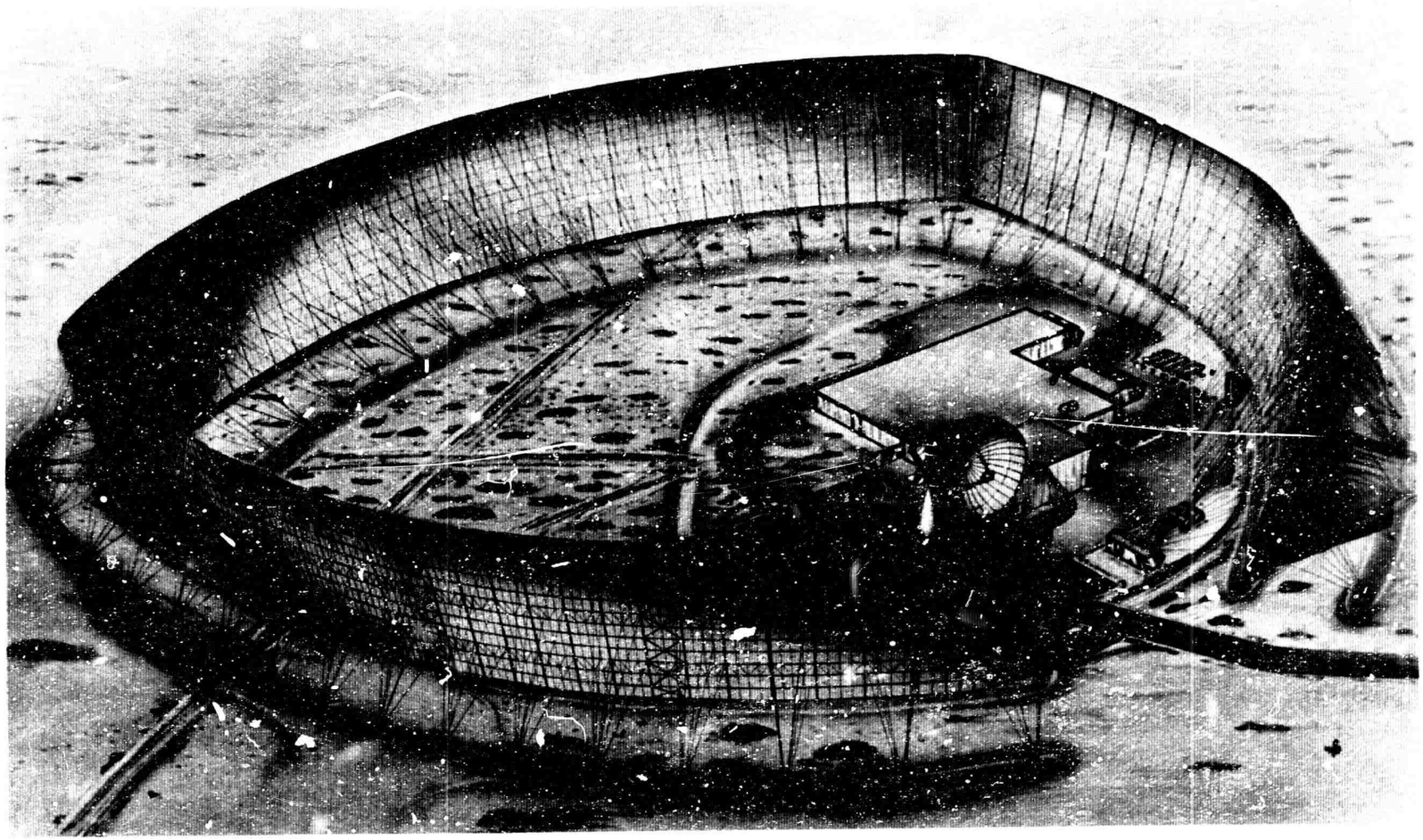

AMRAD ground-clutter shield.

RADAR GROUND-CLUTTER SHIELDS

I. INTRODUCTION

Recently there has been interest[1,2] in the use of metal fences or shields to reduce the ground clutter received by a radar located in mountainous terrain. This report considers the design of a clutter shield for an L-band ($\lambda = 0.75$ ft) radar employing a 60-ft parabolic reflector with a Cassegrainian geometry and with a mean antenna height of 58 ft.

Investigation of the problem was initiated in October 1963 when a series of working papers[3] were prepared. An experimental scale-model program was also started to determine the wide-angle side-lobe characteristics of the radar antenna, especially primary feed spillover and feed support scatter. This effort was coordinated with on-site clutter measurements and with the topographic clutter-source distribution.

In addition, a study contract was negotiated with the Wheeler Laboratories[4] who had prior experience in the design of radar fences for various Bell Telephone Laboratories projects.

Finally, the effect of the shield on a scale model of the radar antenna was experimentally determined and the structural parameters were specified.

II. THEORETICAL DISCUSSION

A. Simple Knife-Edge Diffraction

The field behind a metal obstacle or straight edge is a classic problem in physical optics which was solved rigorously by Sommerfeld in 1896.

Consider the geometry of a shield of height h with a clutter echo arriving at an angle α, as shown in Fig. 1. The field[5] near the geometric shadow (for either polarization) at height g and distance d is given by

$$E(g,d) = \frac{e^{-j(\pi/4)}}{\sqrt{2}}\, e^{jkr\cos(\gamma-\alpha)} \left\{\left[\frac{1}{2} - C(w)\right] + j\left[\frac{1}{2} - S(w)\right]\right\} \qquad (1)$$

where

$$w = 2\sqrt{\frac{2r}{\lambda}}\,\sin\frac{(\gamma-\alpha)}{2}$$

$$C(w) = \int_0^w \cos\frac{\pi}{2}\tau^2 d\tau$$

$$S(w) = \int_0^w \sin\frac{\pi}{2}\tau^2 d\tau$$

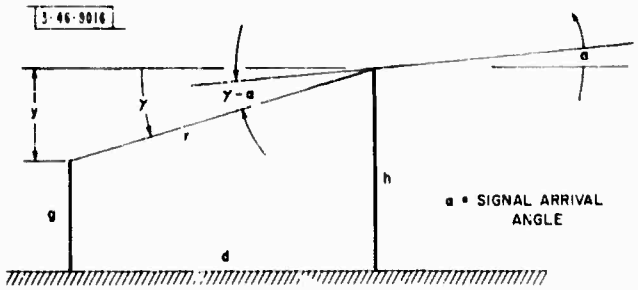

Fig. 1. Fence geometry.

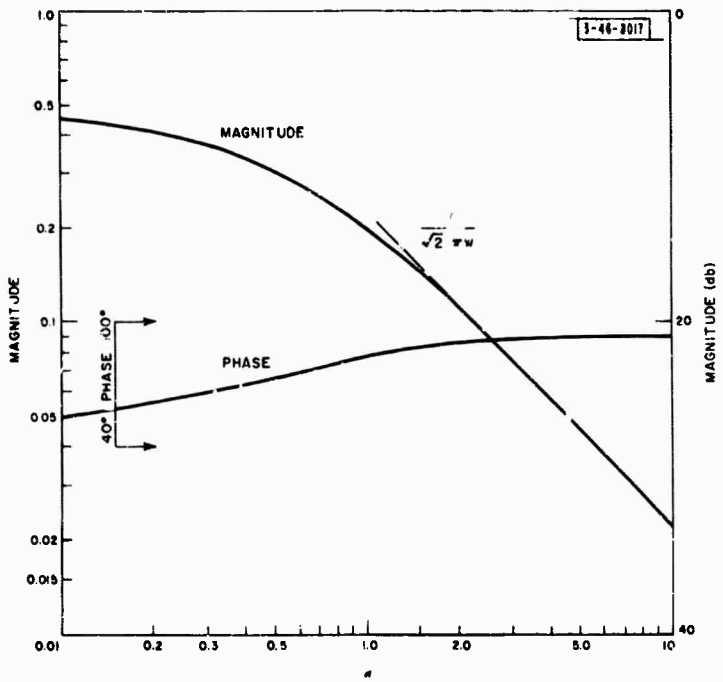

Fig. 2. Diffraction function.

The functions C(w) and S(w) are the Fresnel integrals and have been extensively tabulated.[6] Since the field in the shadow region has a rapidly varying phase characteristic, it is preferable to introduce the auxiliary functions,[7] defined for $w > 0$, by

$$e^{j(\pi/2)w^2}\,[g(w) + jf(w)] = [\tfrac{1}{2} - C(w)] + j[\tfrac{1}{2} - S(w)] \quad . \tag{2}$$

The oscillatory nature of Eq. (1) has been factored out and the auxiliary functions g(w) and f(w) have a monotonically decreasing behavior.

In the shadow region, where $w > 0$, Eq. (1) becomes

$$E(g,\alpha) = \frac{e^{j[kr-(\pi/4)]}}{\sqrt{2}}\,[g(w) + jf(w)] = D(w)\,e^{j[kr-(\pi/4)]} \tag{3}$$

where the field diffraction function is defined as

$$D(w) = \frac{1}{\sqrt{2}}\,[g(w) + jf(w)] \quad . \tag{4}$$

Its magnitude and phase are plotted in Fig. 2. Similarly, in the illuminated region $w < 0$ and Eq. (1) can be rewritten as

$$E(g,\alpha) = e^{jkr\cos(\gamma-\alpha)} - \frac{e^{jkr}}{\sqrt{2}}\,[g(-w) + jf(-w)]\,e^{-j(\pi/4)} \quad . \tag{5}$$

Equations (3) and (5) indicate that the field beyond the fence is:

(1) In the shadow region, a cylindrical wave originating at the top of the straight edge and proportional to the diffraction function Eq. (4). An observer here would see an illuminated line source at the fence edge.

(2) In the illuminated region, the original incident field plus a disturbing field diffracted from the fence edge.

Figure 3 shows the vertical field distribution at a distance of 500 ft at a wavelength of 0.75 ft and for zero clutter arrival angle. Note that:

(1) Above the fence, the field is slightly perturbed.

(2) At the geometric shadow, the field is 6 db down.

(3) Below the fence, the field decreases rapidly at first and then more slowly; however, the phase increases rapidly.

The horizontal axis of the AMRAD radar is 58 ft above the ground and the antenna aperture rotates on a 31-ft moment arm. The aperture center, therefore, rises about 10 ft at a typical target-tracking angle of 20°. This movement of the aperture center, the primary feed horn and the aperture edges is shown in Fig. 4.

Figure 5 shows the fence attenuation at the aperture center for various fence heights and fence distances when the radar is elevated to 20°. Although the actual clutter signal received is an aperture-integrated effect, for the present, the center aperture field may be taken as a measure of the fence clutter rejection. The received field is strongly biased toward this value by the aperture illumination taper and by the circular aperture shape. Furthermore, antenna pattern measurements indicated that a major portion of the side-lobe structure was caused by forward spillover from the centrally located primary feed.

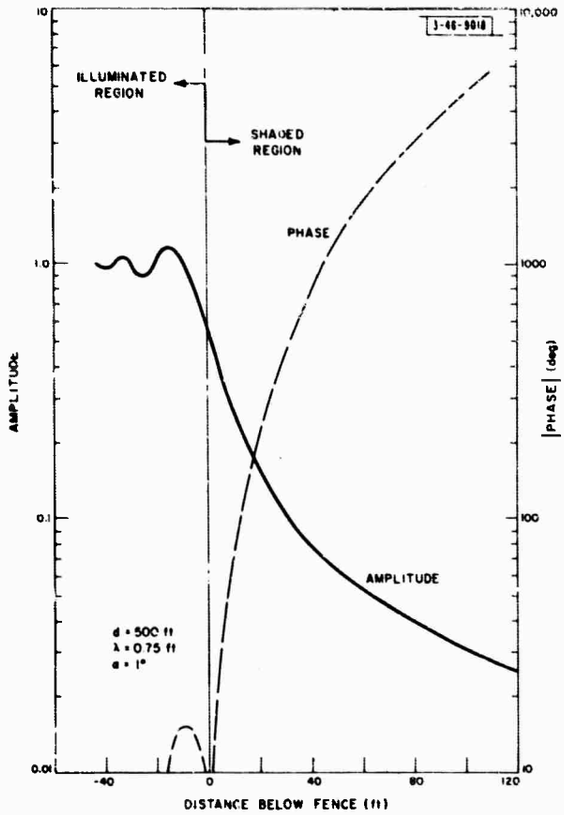

Fig. 3. Calculated knife-edge diffraction.

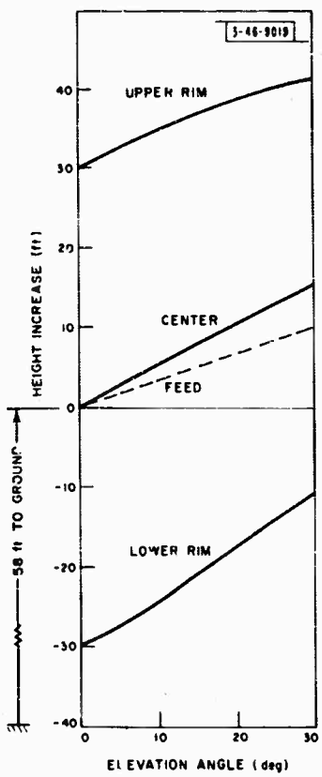

Fig. 4. Effect of dish offset from horizontal axis.

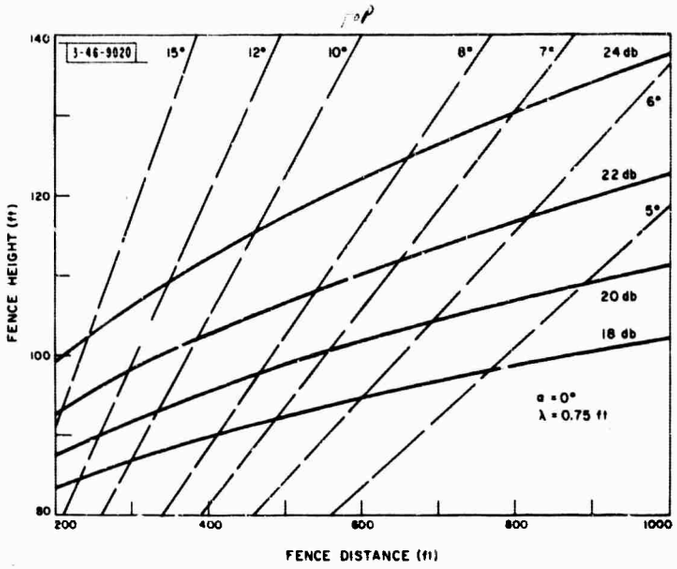

Fig. 5. Calculated one-way clutter reduction and minimum unobstructed tracking angle (elevation angle 20°).

Figure 5 also shows the minimum unobstructed target-tracking angle defined as that elevation angle where the antenna aperture beam cylinder is just tangent to the top edge of the fence. As the shield is in the near field of the radar, further depression will affect the radiation patterns. This situation is considered in Sec. II-D.

It is evident from Fig. 5 that, to realize high clutter attenuation and low target-tracking angles, the shield must be high and far away, and therefore expensive. It will also be difficult to achieve a one-way clutter rejection greater than approximately 20 to 24 db with a reasonable structure.

A trade off among clutter rejection, minimum target angle and fence cost resulted in the selection of a shield 100 ft high at a distance of 500 ft. This theoretically provided a nominal 40-db two-way clutter attenuation and permitted unobstructed target tracking to about 7.8° elevation.

Since the radar has a principal sector of interest, the shield was made triangular instead of circular to economize on fence perimeter and cost. The final configuration is shown in Fig. 6.

To prevent damage to the receiver front end when the antenna beam is depressed onto the shield, the latter is slanted 15° away from the radar.

At first a solid-surface fence was proposed. However, structural considerations led to a mesh surface which is an effective reflector of microwave energy and is frequently used for parabolic reflectors. For clutter rejection application, the energy transmission must be substantially lower than the clutter rejection figure; therefore, a relatively fine mesh, 0.25-in. square with 0.047-in. steel wire, was specified. (The calculated transmission of this size mesh is −30 db.) The mesh was galvanized after weaving, and was firmly attached to the support structure to prevent the generation of any contact noise.

In addition to the reduction of terrain clutter echoes, the shield will provide a slightly lower (approximately 6°K) antenna noise temperature because of the small fraction of energy, previously hitting the ground, now being directed outward by the fence.

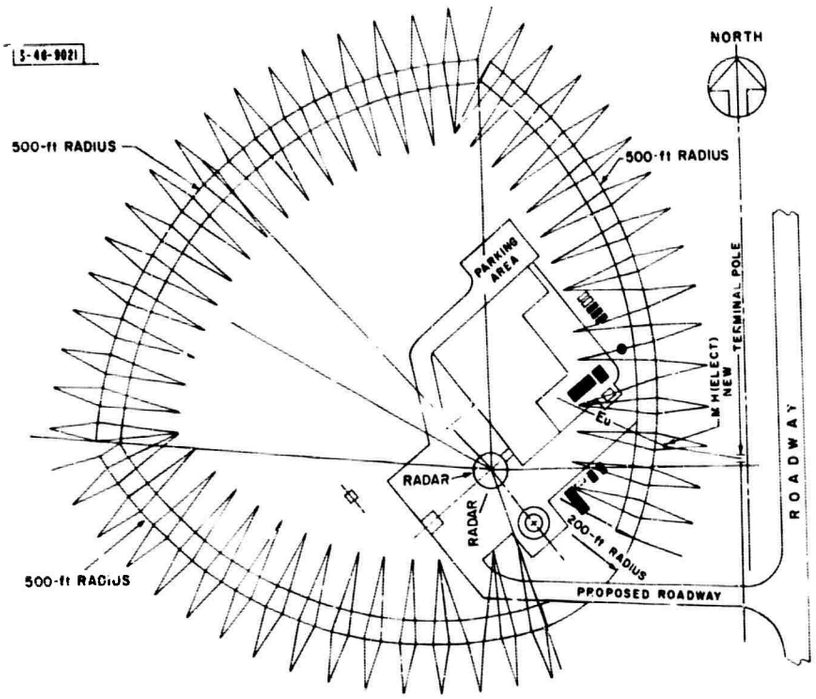

Fig. 6. Fence layout.

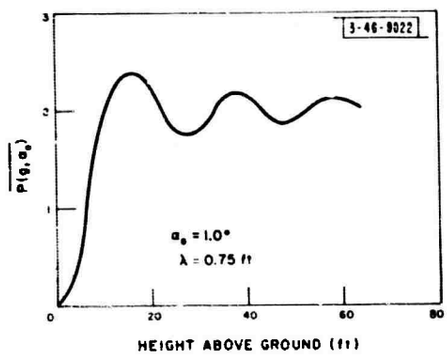

Fig. 7. Vertical power distribution caused by integrated clutter.

In the course of experimental investigation, the straight fence was modeled at a wavelength of 8.57 mm (scale factor 26.7). As the theoretical diffraction curve represents a rigorous solution, an experimental agreement indicates a satisfactory test site (see Sec. III).

B. Integrated Ground Clutter

Radar ground clutter signals form an extended target both in angle of arrival and in range. For a specific range there will be an angular distribution of signals from the horizon to a maximum elevation angle α_o, corresponding to the maximum height of the mountainous terrain.

In addition, clutter arriving at the angle α will also arrive, as a ground reflected wave, at the angle $-\alpha$. The ground reflection coefficient is essentially -1 for either linear polarization because of the small grazing angle.

Without a fence, the field intensity at height g, due to a clutter signal arriving at angle α, may be written

$$E(g,\alpha) = e^{j(2\pi/\lambda)\, g \sin\alpha} - e^{-j(2\pi/\lambda)\, g \sin\alpha} = 2j \sin\left(\frac{2\pi}{\lambda} g \sin\alpha\right) \tag{6a}$$

and the power

$$P(g,\alpha) = 2\left[1 - \cos\left(\frac{4\pi}{\lambda} g \sin\alpha\right)\right] \quad . \tag{6b}$$

This equation shows the familiar sinusoidal distribution with height which would be obtained if the field due to a single clutter element were probed. For an antenna at a given height, certain clutter arrival angles are suppressed and others enhanced because of the ground-reflection effect.

As the actual clutter signal is angularly incoherent, integration can be used to obtain the average power. Assuming that the return is uniformly distributed to some maximum angle α_o,

$$\overline{P(g,\alpha_o)} = \frac{1}{\alpha_o} \int_o^{\alpha_o} P(g,\alpha)\, d\alpha = 2\left[1 - \frac{\sin\left(\frac{4\pi g \sin\alpha_o}{\lambda}\right)}{\frac{4\pi g \sin\alpha_o}{\lambda}}\right] . \tag{7}$$

With an angular spread of clutter signals, the vertical energy distribution is no longer sinusoidal but rapidly approaches a constant value. This is shown in Fig. 7 and indicates that an antenna, well off the ground, is subject to an essentially constant clutter field.

When a fence of height h is introduced, the clutter field becomes

$$E(g,\alpha) = \frac{e^{jkr}}{\sqrt{2}} \left\{[g(w_1) + jf(w_1)]\, e^{-jkhr \sin\alpha} - [g(w_{-1}) + jf(w_{-1})]\, e^{jkhr \sin\alpha}\right\} \tag{8}$$

the power is

$$\begin{aligned} P(g,\alpha) = {} & \frac{[g^2(w_1) + f^2(w_1)] + [g^2(w_{-1}) + f^2(w_{-1})]}{2} \\ & - [g(w_1)\, g(w_{-1}) + f(w_1)\, f(w_{-1})] \cos(2kh \sin\alpha) \\ & + [f(w_1)\, g(w_{-1}) - g(w_1)\, f(w_{-1})] \sin(2kh \sin\alpha) \end{aligned} \tag{9}$$

where

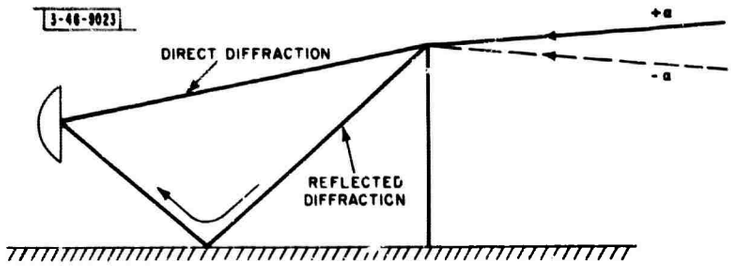

Fig. 8. Ground reflection geometry.

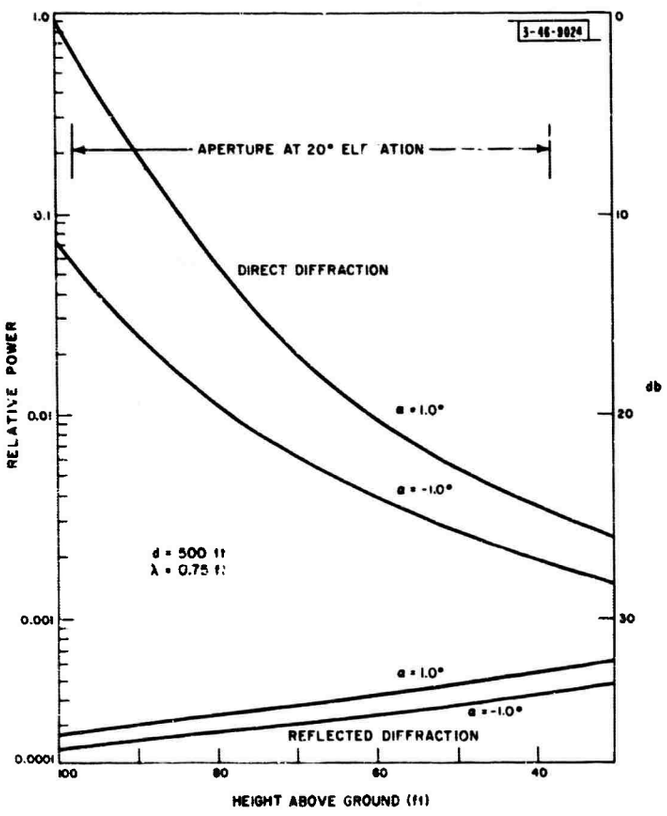

Fig. 9. Comparison of foreground reflected waves.

$$w_1 = 2\sqrt{\frac{2r}{\lambda}}\sin\frac{\gamma-\alpha}{2}$$

$$w_{-1} = 2\sqrt{\frac{2r}{\lambda}}\sin\frac{\gamma+\alpha}{2}$$

$$w_o = 2\sqrt{\frac{2r}{\lambda}}\sin\frac{\gamma}{2} \quad .$$

As the auxiliary functions g(w) and f(w) are well behaved and slowly varying, their arithmetic and geometric means can as a first approximation be replaced by their average values

$$P(g,\alpha) \doteq [g^2(w_o) + f^2(w_o)]\,[1 - \cos(2kh\sin\alpha)] \quad . \tag{10}$$

The field now is independent of he antenna height g (except as determined by the diffraction function factor). For certain clutter angles, determined now by the fence height, the entire field is enhanced or, to the approximation made, vanishes.

As in Eq. (7), the angularly integrated clutter can be written

$$\overline{P(g,\alpha_o)} = [g^2(w_o) + f^2(w_o)]\left[1 - \frac{\sin(2kh\alpha_o)}{(2kh\alpha_o)}\right] \tag{11}$$

where the integrated field, for large fence heights, approaches the zero-angle-of-arrival diffraction function.

Note that the field does not vanish on the ground surface; this is because all the waves behind the fence have not been included. Another spectrum of waves is diffracted by the fence edge and reflected from the ground immediately in front of the antenna. This series of waves, due to the larger diffraction angle, is considerably weaker than that diffracted directly into the antenna by the fence edge. The two series of waves are presented in Fig. 8.

Figure 9 shows the range of the two fence-diffracted waves as the arrival angle ranges from $\alpha = \pm 1°$ for the 100-ft fence at a distance of 500 ft. Note that the foreground reflected waves are about 15 db weaker due to their larger diffraction angle. In addition, these waves will not be reflected completely from the foreground, as the incident angle is about 10°. Finally, at a typical antenna tracking angle of 20°, these waves arrive about 30° from the beam axis and will be further attenuated. For these reasons, the foreground diffracted waves are neglected in further calculations.

C. Fence Edge Treatment

1. Simple Serrations

In the early stages of the AMRAD program, the possibility existed that greater clutter suppression was necessary than the nominal 20 db obtainable from a simple fence of reasonable size. A number of suggestions have appeared in the literature[8-10] to reduce the shadow field behind an edge or disk. These have included edge serrations, thick edges, properly located holes or slots, and phase-changing tubes. Structurally, the edge serration appeared to be the simplest for this application and was first investigated by Wheeler Laboratories both theoretically and experimentally.[4]

Basically, the method consists of making sections of the shield at two or more different heights, so that the path lengths to the region of interest differ by a half wavelength and the

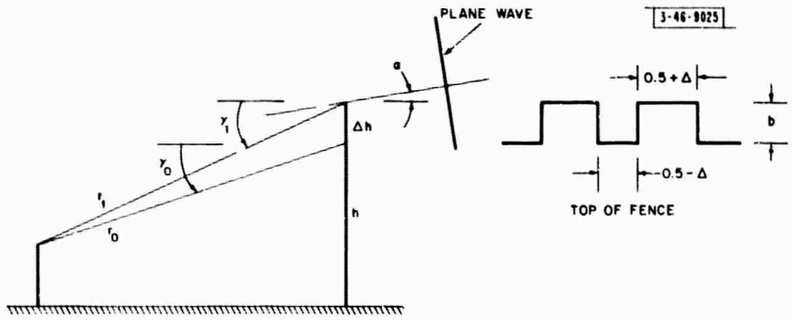

Fig. 10. Serration geometry.

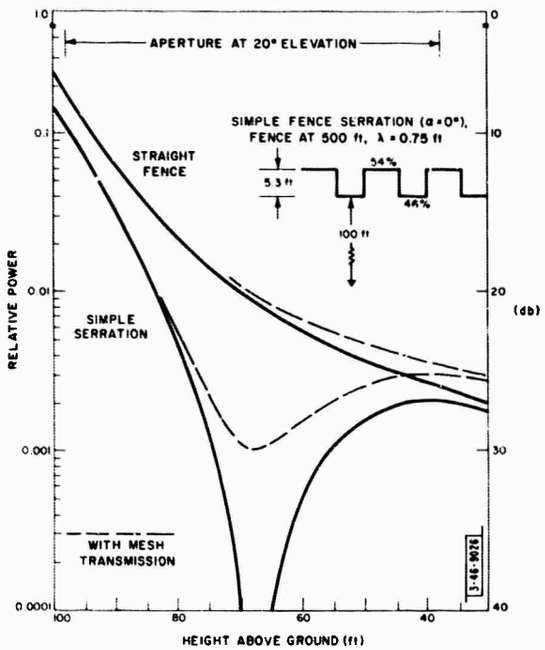

Fig. 11. Calculated vertical field distribution behind serrated fence.

field is essentially canceled in this region. By further adjusting the serration widths, complete cancellation is theoretically possible at a selected point. A fence serration geometry is shown in Fig. 10.

For the simplest, or two-height serration, the field may be written, from Eq. (3), by superposition

$$E(g,\alpha) = (0.5 - \Delta)\,\frac{e^{jkr_o}}{\sqrt{2}}\,[g(u_o) + jf(u_o)]$$

$$+ (0.5 + \Delta)\,\frac{e^{jkr_1}}{\sqrt{2}}\,[g(u_1) + jf(u_1)]\; e^{-jk\Delta h \sin\alpha} \qquad (12)$$

where

$$u_o = 2\sqrt{\frac{2r_o}{\lambda}}\,\sin\frac{\gamma_o - \alpha}{2}$$

$$v_1 = 2\sqrt{\frac{2r_1}{\lambda}}\,\sin\frac{\gamma_1 - \alpha}{2} \quad .$$

As the clutter signal and its ground reflection arrive symmetrical to the horizon, the serration depth is chosen for cancellation at the antenna center for a horizontally arriving signal.

Figure 11 shows the calculated field distribution for the serrated fence compared to the straight-edge fence. Cancellation was chosen at 68 ft above ground (antenna center for a 19° tracking angle). A complete null will not be realized because the mesh transmission sets a 30-db limit. In addition, for other clutter arrival angles the null shifts up or down along the aperture about 8.7 ft per degree. This effect is shown in Fig. 12 where the contributions for $\alpha = -1°$, $0°$, and $+1°$ have been added incoherently. These clutter contributions have been weighted 0.5, 1.0 and 0.5. Comparison is made, in Fig. 12, with the knife edge computed on the same basis. Finally, the neglected foreground reflected waves, about 35 db down (see Fig. 9), and other leakages will set a limit to the obtainable suppression.

2. Double Serrations

The serration principle can be extended to more than a single step. By increasing the number of serration steps, the region of low response can be increased in width. The idea is similar to that of stagger tuning in electrical circuits. Figure 13 shows the field distribution of a two-step serration. Here, in theory, a 27-db one-way suppression (including mesh transmittivity) is obtained over the central 30-ft region of the circular aperture.

The problem still exists of determining the response of the large 60-ft aperture, when elevated to a typical tracking angle, to this complex clutter field. Because of the significant direct pickup of the centrally located Cassegrainian primary feed, this was resolved by scale-model measurements.

The first edge treatment investigated at Lincoln Laboratory, at a frequency scale factor of 26.7, was the stagger-tuned arrangement shown in Fig. 13. The experimental vertical field distributions were extremely disappointing. Further probing of the field in the horizontal plane, at the level of expected cancellation, revealed periodic oscillations of large amplitude. Clearly, the simple analysis based on Eq. (12) was inadequate.

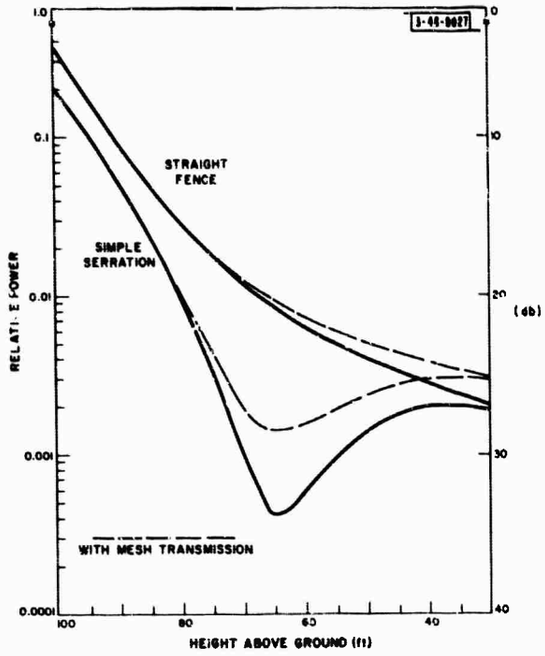

Fig. 12. Effect af incoherent addition of clutter signals arriving at angles af ±1° and 0°.

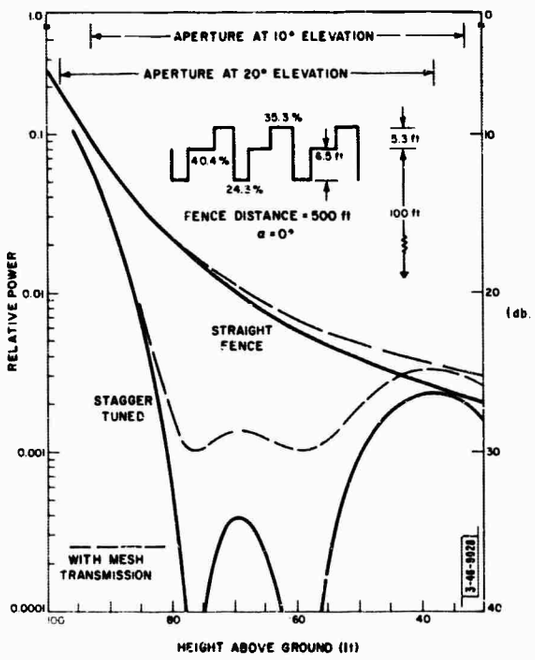

Fig. 13. Calculated vertical field distribution for stagger-tuned fence.

3. Serration "Resonance"

Before embarking on a mathematical derivation, it is well to explain the source of the difficulty by means of physical reasoning. Consider a point P at distance d behind the fence and y below the edge. To an observer at P, the top of the serrated fence appears as a line source with a square-wave phase function $\varphi(x)$, as shown in Fig. 14. The radiation arriving at P is further delayed by the increased path length to each section.

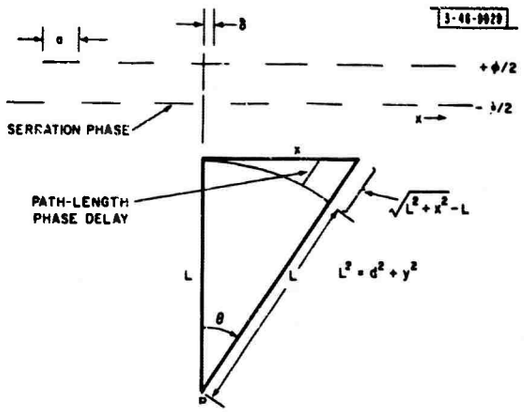

Fig. 14. Phase contributions at general point P.

When the observer is at the cancellation level, where $\varphi = \pi$, the edge appears as a series of out-of-phase sections. The contribution from the central region essentially vanishes. However, the square-wave phase function can be represented as a staircase function where each step is π radians, as shown in Fig. 15(a). When the slope of the indicated path-length delay is equal and opposite to the staircase slope, that region of the edge will appear in phase to the observer and may create a substantial field. Additional sets of resonant regions may be found by considering equivalent staircase functions having larger slopes where each step is 3π, 5π, etc.

One additional feature of the field can be predicted from physical reasoning. The alternating phase function $\varphi(x)$ leads to an oscillatory field as the observer moves parallel to the shield (increasing δ in Fig. 14). This can be seen by taking the origin ($x = 0$) at the edge of a step. The function $\varphi(x)$ is odd and contributes zero signal at P. Now, if the observation point is moved so $\delta = a/2$, the function $\varphi(x)$ is even and the resonance pair is in phase to contribute a maximum signal. Maxima are therefore separated by the serration width a.

Further insight is given by an equivalent approach utilizing Fresnel zones. Figure 15(b) shows a few Fresnel zones drawn on the fence from the observation point P. The lower part of the figure is obtained for $y = 0$, while the upper part is obtained when P is at the cancellation region. Interesting behavior occurs where the width of the Fresnel zones is equal to the serration width. The contribution of the slots is then seen to be in phase at P, and a resonant (or stationary-phase) region exists. Higher order resonances occur where there are 3, 5, . . ., Fresnel zones in a serration width.

Examination of the geometry leads to the conclusion that the interference of the first-order resonant regions creates an oscillatory field of a period equal to that of the serrations as P moves in a direction parallel to the fence edge. This analysis can be extended to multiple-step serrations. For example, in the case of the double serrations shown in Fig. 13, the first-order stationary-phase region occurs where there are two Fresnel zones per period of serrations.

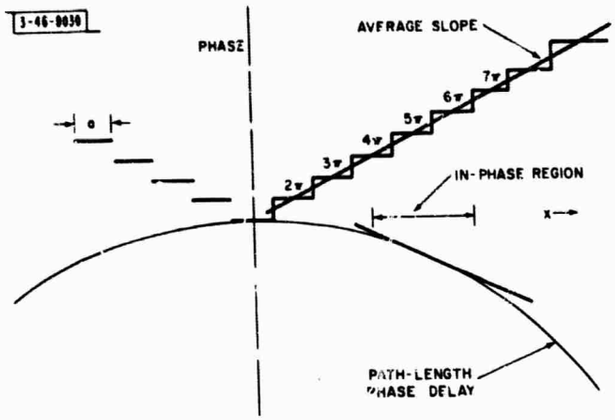

(a) Phase at cancellation level.

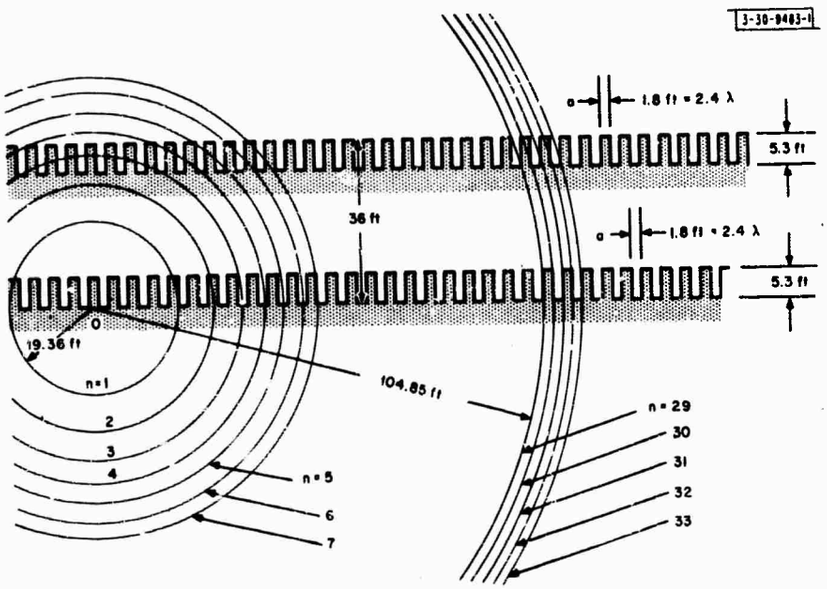

(b) Fresnel zones on fence.

Fig. 15. Constructions for explaining serration resonance.

4. Mathematical Derivation

By suppressing the edge-diffraction function and assuming equal-amplitude contributions from adjacent sections of the serrated shield, the field at P may be written for the geometry of Fig. 14 as

$$e(\varphi,\alpha) = \int_{-S}^{S} O(\Theta)\, \frac{\exp[j(2\pi/\lambda)(\sqrt{L^2 + x^2} - L)]}{\sqrt{L^2 + x^2}}\, e^{j\varphi(x)}\, dx \qquad (13)$$

where

$2S$ = the total length of the shield

$O(\Theta)$ = an obliquity function which may be taken as $\cos\Theta$

$\varphi(x) = \frac{\varphi}{2}\,(-1)^n$

and

$$e^{j\varphi(x)} = \cos\frac{\varphi}{2} + j(-1)^n \sin\frac{\varphi}{2}$$

where n takes integer values equal to the serration number as x increases. The square-wave function $(-1)^n$ may be written by Fourier series expansion:

$$f(x) = (-1)^n = \frac{4}{\pi} \sum_{m=o}^{\infty} \frac{(-1)^m}{(2m+1)} \cos(2m+1)\frac{\pi}{a}(x+\delta) \quad .$$

Substituting in Eq. (13) and neglecting constant factors,

$$e(\varphi,\alpha) = \int_{-S}^{S} \frac{\exp[j(2\pi L/\lambda)\sqrt{1 + (x^2/L^2)}]}{1 + (x^2/L^2)} \times \left[\cos\frac{\varphi}{2} + j\frac{4}{\pi}\sin\frac{\varphi}{2} \sum_{m=o}^{\infty} \frac{(-1)^m}{(2m+1)} \cos(2m+1)\frac{\pi}{a}(x+\delta)\right] dx \quad . \qquad (14)$$

The integral may be evaluated by the method of stationary phase where, for large t,

$$\int_{-S}^{S} g(x)\, e^{jth(x)}\, dx = \sqrt{\frac{\pi}{2}}\, g(x_o)\, \frac{\exp\{j[th(x_o) \pm (\pi/4)]\}}{\sqrt{th''(x_o)}} \qquad (15)$$

where x_o is the stationary phase point in the integration interval.

The first term of Eq. (14) has a stationary point at x = 0, and the remaining terms have symmetric sets of points located at

$$x_o = \frac{\pm L(2m+1)\lambda/2a}{\sqrt{1 - [(2m+1)\lambda/2a]^2}} \quad . \qquad (16)$$

The field at P can then be written, neglecting constants

$$e(\varphi,\alpha) = \cos\frac{\varphi}{2}\, e^{j(2\pi L/\lambda)} + j\frac{8}{\pi}\sin\frac{\varphi}{2} \sum_{m=o}^{\infty} \frac{(-1)^m}{(2m+1)} \left\{1 - \left[\frac{(2m+1)\lambda}{2a}\right]^2\right\}^{1/4} \times \cos(2m+1)\frac{\pi}{a}\delta\, \exp\{j(2\pi L/\lambda)\sqrt{1 - [(2m+1)\lambda/2a]^2}\} \qquad (17)$$

e first term of Eq. (17) represents the contribution of the edge in-phase components which v at the cancellation level where $\varphi = \pi$. The summation terms are the contribution of the undesired resonant regions; their angular position is shown in Fig. 16, which is plotted from Eq. (16). Since we desire to eliminate these regions, we need consider the location of the first region only. This occurs for $m < 1$, and the length of fence 2S satisfies

$$S < \frac{(3\lambda/2a)\, L}{\sqrt{1-(3\lambda/2a)^2}} \tag{18}$$

in which case Eq. (17) becomes

$$e(\varphi,\alpha) = \cos\frac{\varphi}{2}\, e^{j(2\pi L/\lambda)} \quad j\frac{8}{\pi}\sin\frac{\varphi}{2}\left\{\left[1-(\lambda^2/4a^2)\right]^{1/4}\cos\frac{\pi\delta}{a}\right\}$$

$$\times \exp\left[j(2\pi L/\lambda)\sqrt{1-(\lambda^2/4a^2)}\right] \quad . \tag{19}$$

If the field is probed horizontally, we measure the power

$$P(\varphi,\alpha) = \cos^2\frac{\varphi}{2} + \left(\frac{8}{\pi}\right)^2 \sin^2\frac{\varphi}{2}\left\{\left[1-(\lambda^2/4a^2)\right]^{1/2}\cos^2\frac{\pi}{a}\,\delta\right\}$$

$$+ \frac{16}{\pi}\sin\frac{\varphi}{2}\cos\frac{\varphi}{2}\left\{\left[1-(\lambda^2/4a^2)\right]^{1/4}\cos\frac{\pi}{a}\,\delta\right\}\sin\left\{\frac{2\pi L}{\lambda}\left[1-\sqrt{1-(\lambda^2/4a^2)}\right]\right\} \quad . \tag{20}$$

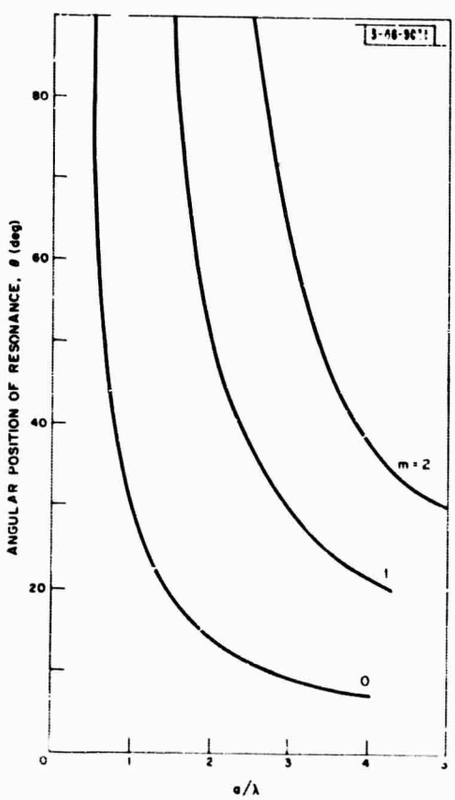

Fig. 16. Location of stationary phase points on serrated fence.

On the basis of this approximate analysis we find that, at various levels below the edge, the horizontally probed field exhibits different behaviors.

(a) At the level of the edge, where $\varphi = 0$, or if the edge is not serrated,

$$P(0,\alpha) = 1 \tag{21}$$

or no horizontal dependence.*

(b) At the expected serration cancellation level, where $\varphi = \pi$,

$$P(\pi,\alpha) = \left(\frac{8}{\pi}\right)^2 \left[1 - (\lambda^2/4a^2)\right] \cos^2 \frac{\pi}{a} \delta \quad . \tag{22}$$

Note that there are complete nulls with a spacing equal to a (the serration width). For only one undesired resonance, a/λ varies between approximately 1 and 2 (Fig. 16), and the maximum field is almost 8 db higher than if there were no serration. Furthermore, the existence of this horizontally periodic field at the cancellation level is a definite indication of the presence of the undesired resonant region on the fence edge. However, to measure this field properly, a nondirective probe must be used to respond to the off-axis sources.

(c) At an intermediate level, the field also has interesting behavior. Since the last factor of the last term of Eq. (20) has an oscillatory behavior, its limiting values are approximately

$$P(\varphi,\alpha) \simeq \cos^2 \frac{\varphi}{2} + \left(\frac{8}{\pi}\right)^2 \sin^2 \frac{\varphi}{2} \cos^2 \frac{\pi}{a} \delta \pm 2 \left(\frac{8}{\pi}\right) \times \sin \frac{\varphi}{2} \cos \frac{\varphi}{2} \cos \frac{\pi}{a} \delta$$

$$P(\varphi,\alpha) \simeq \left[\frac{8}{\pi} \sin \frac{\varphi}{2} \cos \frac{\pi}{a} \delta \pm \cos \frac{\varphi}{2}\right]^2 \quad .$$

At a vertical level, where $\tan(\varphi/2) = \pi/8$,

$$P(\varphi,\alpha) \simeq \cos^2 \frac{\varphi}{2} \left[1 \pm \cos \frac{\pi}{a} \delta\right]^2 \simeq \begin{cases} 4 \sin^4 \left(\frac{\pi}{2a} \delta\right) \\ 4 \cos^4 \left(\frac{\pi}{2a} \delta\right) \end{cases} . \tag{23}$$

In other words, the spacing between nulls is now 2a, or twice the cancellation level period.

To eliminate these off-axis resonant regions, it is necessary to make the serration width small. From Fig. 16 it is seen that a width less than $\lambda/2$ is required for a fence of infinite length; whereas, for a screen where S = L, a width less than $\lambda/\sqrt{2}$ is necessary.

An analysis similar to that performed for the straight shield above can be set up for a circular shield. The general results are similar, and the angular position of the first resonant region is now given by

* Actually, at no level are the contributions from adjacent sections of the serrated fence exactly equal in both amplitude and phase. Small oscillations are therefore always expected.

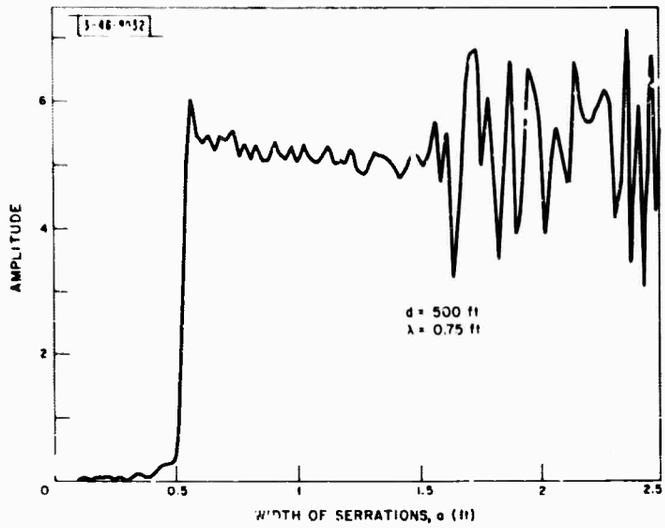

Fig. 17. Computed curve giving field at cancellation region vs serration width.

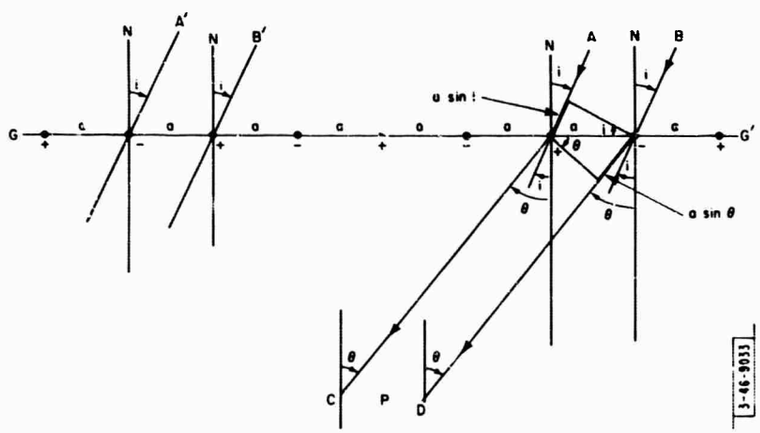

Fig. 18. Geometry for grating-lobe calculation.

$$\sin\Theta_o = \frac{\lambda}{2a} \tag{24}$$

or identical to Fig. 16.

5. Computer Analysis

Prior to the mathematical analysis, the original basic equation (13) was programmed. As machine computation is a summation, the contribution of each step was summed according to

$$\sum_n (-1)^n \frac{\sin(\pi a/\lambda)\,\Theta_n}{(\pi a/\lambda)\,\Theta_n} \cdot \frac{\exp[j(2\pi/\lambda)(\sqrt{L^2 + n^2a^2} - L)]}{\sqrt{L^2 + n^2a^2}} \tag{25}$$

The summation was carried out over the entire length of the fence as a function of the serration width. The result for the field at the cancellation level is shown in Fig. 17 for the case where L = S. There is a negligible signal for serration widths less than $\lambda/\sqrt{2}$, a rapid increase at this point when the first resonance appears at the far end of the shield, and a constant level until the next resonant region appears at a width $a = 3\lambda/\sqrt{2}$. For larger widths, both resonant regions are present and, due to their different path lengths, beat with each other and form a "standing-wave" pattern as a is varied. Since the relative contributions of the various resonant regions are in the ratio of the coefficients of a square-wave Fourier expansion, namely 1 to $\frac{1}{3}$, the expected SWR of 2:1 is confirmed by Fig. 17.

Although this computation was made early in the program, the result was not completely understood until the mathematical analysis was made. The field behind the fence also proved to be more complex than would have been predicted by simple array grating-lobe theory.

6. Grating-Lobe Approach

Additional insight into the horizontal plane behavior of the serrations may be gained by considering them as constituting a one-dimensional transmission grating. At the level corresponding to the cancellation region, the grating elements must be taken as alternating in sign. Figure 18 shows such a grating with rays A and B incident at angle i. The emerging rays C and D will add in phase at angle Θ when the combined path length difference and alternating sign of the elements satisfy the condition

$$\frac{2\pi}{\lambda}(a\sin\Theta - a\sin i) \pm \pi = \pm 2n\pi \tag{26}$$

Grating lobes will therefore occur when

$$\sin\Theta = \left[\pm\frac{(2n+1)}{2a}\frac{\lambda}{} + \sin i\right] < |1| \quad (n = 0,1,2,3,\ldots) \tag{27}$$

For normal incidence i = 0, and Eq. (27) gives the same information found in Fig. 16. Since the observation point P is located symmetrically in the near field of the grating, the "grating lobes" would appear symmetrically on the fence as "resonant" regions. P would then be in the far field of each resonant region.

The effect of off-axis signals (i > 0) is to reduce the effectiveness of the serrations, since the position of one of the resonant regions shifts toward the center of the fence. Consider, for example, a straight fence with simple serrations of width $a = 0.65\lambda$. Grating lobes occur at ±50.25° for normal incidence. If such a fence is sufficiently short so it intercepts an angle

somewhat smaller than 2 × 50.25° = 100.5° at P, no resonant regions would be observed. However, if the angle of incidence is now changed to +22.65°, Eq. (27) shows that a resonant region would appear at −22.65°, the direct signal at +22.65° being effectively suppressed. Figure 19 illustrates this behavior for all angles of incidence. To avoid all resonant regions for any oblique angle of incidence, the serration width must be less than λ/4 if the directivity of the slot is neglected.

The round fence can be treated in a similar way, but here the effective angle of incidence takes on the full range of values from 0° to 90° for any fence radius. Consequently, grating lobes will always exist, unless a < λ/2. For the above example, where a = 0.65λ, the incident wave would be effectively suppressed, only to appear again as a pair of resonances at ±50.25° to its original direction.

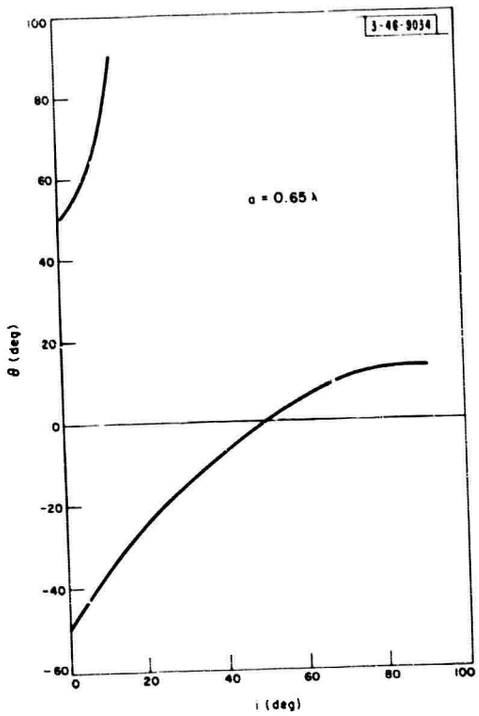

Fig. 19. Grating-lobe angle θ vs angle of incidnece i.

D. Tracking with Fence Obscuration

The effect of the fence on the radar tracking performance is also of interest. As the antenna is depressed from a high elevation angle, it is subject to an interfering field scattered from the edge of the fence. This effect is similar to the normal radar tracking error due to a ground-reflected wave. However, it is smaller, since at grazing angles the ground-reflected wave is about the same strength as the direct wave, whereas the fence-edge diffraction is at least 6 db down. Therefore, as long as the antenna beam cylinder is clear of the fence edge, the tracking error caused is not serious.

At the other extreme is the case where the entire antenna aperture is in the fence shadow. Here the antenna is subject only to the cylindrical wave originating on the fence edge. The radar will track the source of these waves, i.e., the top of the fence, and provide no useful data in elevation angle.

For the geometry under consideration, a large intermediate region exists where the antenna aperture is partially obscured by the shield's geometric shadow. To analyze the tracking problem, we consider, for simplicity, a uniform rectangular aperture half shielded by an "ideal screen." Such a screen is defined as one that creates a geometric shadow step function and is a convenient approximation to the fence-diffracted field.

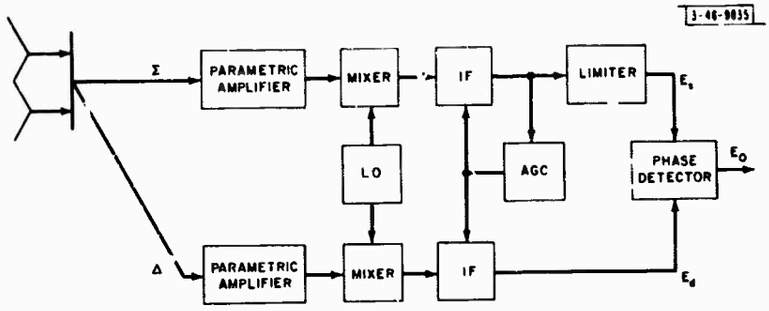

Fig. 20. Tracking circuitry.

A block diagram of the monopulse tracking circuitry is shown in Fig. 20. The signals from the two elevation horns, $g_1(u)$ and $g_{-1}(u)$, are fed into a microwave hybrid. The outputs are the sum and difference signals

$$\Sigma = g_1(u) + g_{-1}(u) \tag{28}$$

$$\Delta = g_1(u) - g_{-1}(u) \tag{29}$$

Since this is an amplitude-sensing monopulse system, $g_1(u)$ and $g_{-1}(u)$ represent two off-axis beams, each being formed by the entire aperture. To explain the half-obstructed case, it is useful to write $g_1(u)$ and $g_{-1}(u)$ in a form showing the contribution of each half of the aperture. Mathematically, the horn outputs, referred to the center of the aperture, are:

Unobstructed Case

$$g_1(u) = \left[\frac{e^{j[(u+u_o)/2]}}{2} + \frac{e^{-j[(u+u_o)/2]}}{2}\right] \frac{\sin[(u+u_o)/2]}{(u+u_o)/2}$$

$$= \frac{\sin(u+u_o)}{u+u_o} \tag{30}$$

$$g_{-1}(u) = \left[\frac{e^{j[(u-u_o)/2]}}{2} + \frac{e^{-j[(u-u_o)/2]}}{2}\right] \frac{\sin[(u-u_o)/2]}{(u-u_o)/2}$$

$$= \frac{\sin(u-u_o)}{u-u_o} \tag{31}$$

Half-Shielded Case

$$g_1(u) = \frac{e^{j[(u+u_o)/2]}}{2} \cdot \frac{\sin[(u+u_o)/2]}{(u+u_o)/2} \tag{32}$$

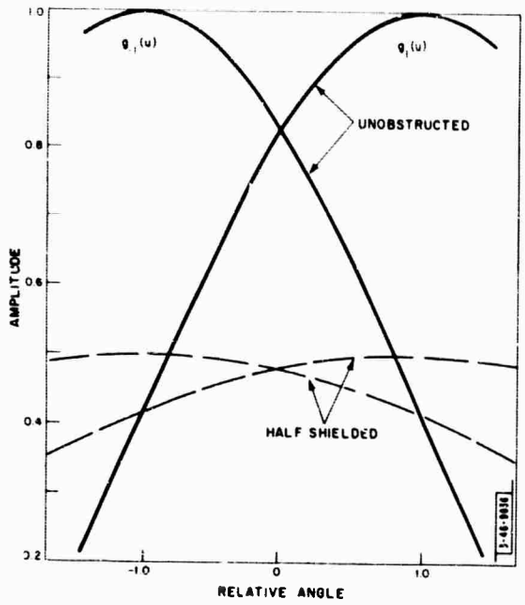

Fig. 21. Calculated individual horn outputs.

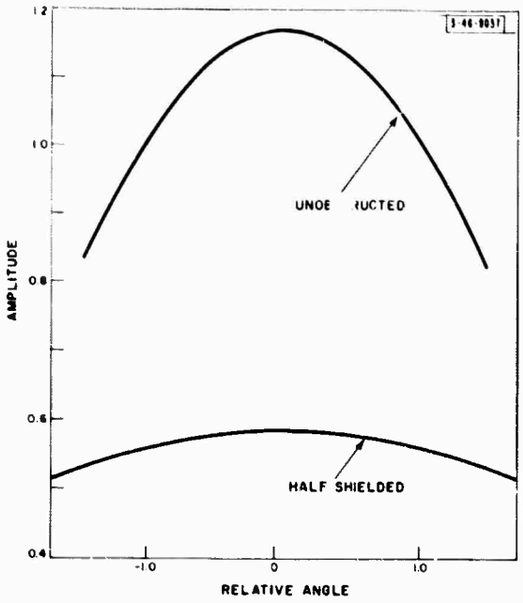

Fig. 22. Calculated output af hybrid sum port.

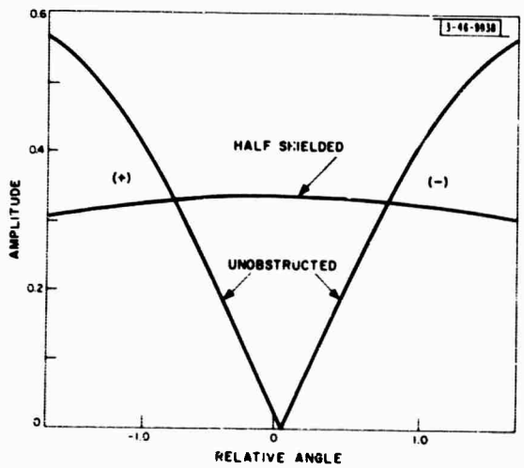

Fig. 23. Calculated output af hybrid difference port.

$$g_{-1}(u) = \frac{e^{j[(u-u_o)/2]}}{2} \cdot \frac{\sin[(u-u_o)/2]}{(u-u_o)/2} \tag{33}$$

where

$$u = \frac{\pi A}{\lambda} \sin\Theta$$

$$u_o = \frac{\pi A}{\lambda} \sin\Theta_o$$

A = rectangular aperture width

Θ_o = beam squint angle

Θ = off-axis angle.

The horn outputs $g_1(u)$ and $g_{-1}(u)$ are plotted in Fig. 21 for the unobstructed and half-shielded cases. The amplitude of the sum and difference is shown in Figs. 22 and 23, respectively. It should be noted that in Fig. 23 the monopulse difference null has disappeared in the half-shielded case, and the general appearance of the difference amplitude function resembles that of the sum.

To examine the operation of the amplitude-sensing monopulse system in the normal and half-shielded cases, reference is again made to Fig. 20. After amplification and coherent mixing, the sum and difference signals are fed through variable gain (AGC) IF amplifiers. Since the AGC is on the sum channel, the output obtained from the difference channel is Δ/E. The signals now pass through a phase-sensitive detector (a multiplier) and a low-pass filter to remove the double-frequency term. The detector output voltage is proportional to[12]

$$E_o = |E_s E_d|^k \cos(\alpha_s - \alpha_d + \alpha_a) = |\Delta|^k \cos(\alpha_s - \alpha_d + \alpha_a) \tag{34}$$

where E_s and E_d are the phase detector inputs, and α_s and α_d are their phases. The term α_a is a phase adjustment provided in the system. The exponent k is the linearity characteristic of the detector which was determined experimentally and is shown in Fig. 24 to be close to unity.

In a normal amplitude-sensing monopulse system, α_s is essentially constant, while α_d varies from zero to π rather sharply when going through boresight. At boresight, the phase difference $(\alpha_s - \alpha_d)$ is equal to $\pi/2$, so α_a is set to zero. When Eq. (34) is evaluated, the result is an error signal which changes sign at boresight, as shown by the solid curve in Fig. 25.

If the aperture is half shielded, both α_s and α_d vary as the target goes through boresight. The phase difference $(\alpha_s - \alpha_d)$ is still equal to $\pi/2$ at boresight, so α_a need not be changed. Evaluation of Eq. (34) yields a reasonable error voltage, as indicated by the dashed curve in Fig. 25.

We have shown that for an "ideal shield" there will be no tracking error. However, because of diffraction effects, there exists a gradual phase change of 45° going from the illuminated to the shadow region. This phase tilt will cause less than a quarter beam-width error. Finally, when the antenna is half shielded, there will be a 6-db loss of antenna gain (12-db two-way).

III. EXPERIMENTAL RESULTS

A. Scale Model

The nominal scale factor of 26.7 was determined by the availability of a narrow-band 1-watt klystron operating at 35 Gcps, which led to a model of manageable size. The choice of a commercially available 30-in. aluminum spinning gave a model dish with a diameter 17-percent

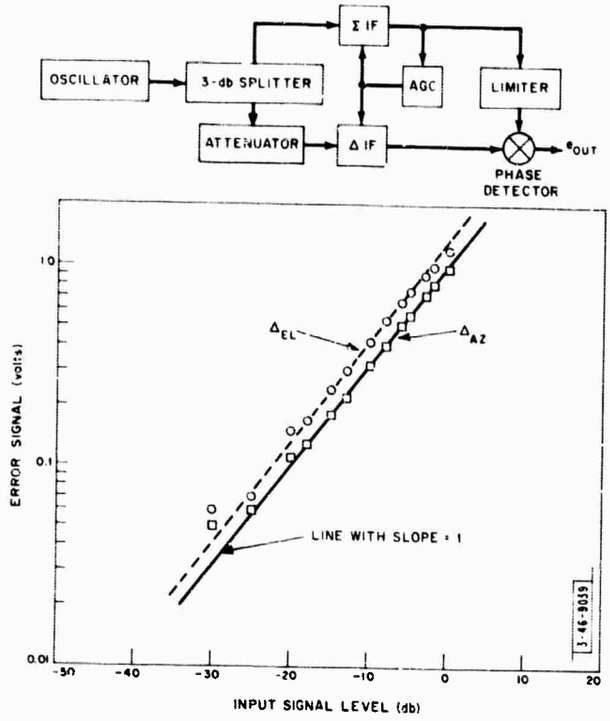

Fig. 24. Measured phase detector characteristics.

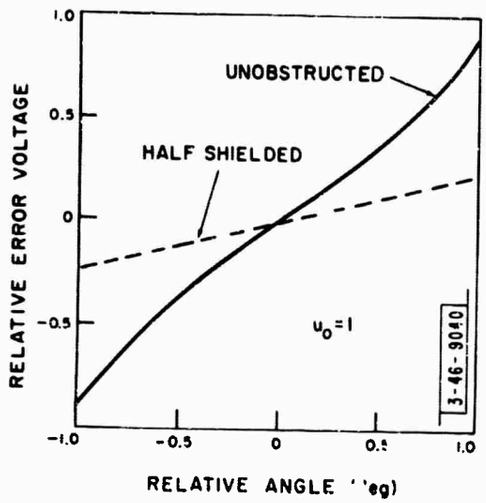

Fig. 25. Calculated error voltage output.

oversize and a focal length 11-percent too long. The desired f/d ratio of 0.25 was consequently reduced slightly. A Cassegrainian geometry was used with a single-horn feed, instead of the actual 4-horn monopulse cluster. This reduced the forward feed spillover past the subreflector, but a great deal remained, as became evident from the secondary patterns. The dish was mounted on the test pedestal at a faithfully scaled offset from the elevation axis.

The model fence was about 7 ft high due to the particular test site topography (Fig. 26). Its effective height, relative to the pedestal's elevation axis, was measured carefully with a surveyor's level. Since the angle of arrival does determine the effective height of the fence, the −0.25° arrival angle at the test site increased the effective model fence height by about 1 in., or about 2.2 ft on the full-size fence. This was taken into consideration when comparing the data with theoretical curves for zero arrival angle.

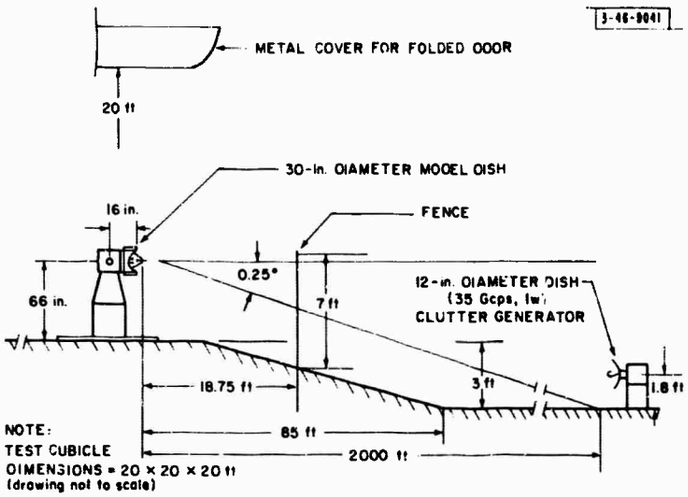

Fig. 26. Geometry of scale-model test site.

The experimental fence consisted of four 8-ft sections of galvanized solid-steel sheet, since a mesh structure was not practical at the scale-model frequency. The required fence distance of 500 ft was scaled down to 18.75 ft, but the total length of 32 ft corresponds to about 850 ft, which exceeds the actual fence length by ±10 ft. Most of the measurements were made on the straight vertical fence, but later a round fence was approximated by placing the four fence sections along chords of the appropriate circle. Both straight and circular fences were temporarily inclined for the purpose of reducing multiple reflections.

B. Test Site

The 2000-ft ground-reflection range at the Lincoln Laboratory Antenna Test Facility was used for all experimental work. A 1-ft transmitter dish, placed near the ground, provided the simulated clutter. Care was necessary in exact adjustment of the transmitter height in order to provide a sufficiently uniform field above the fence. It turned out that the results did not change appreciably when the field intensity tapered down fairly rapidly above the fence edge, as can happen with a ground-reflection range.

Severe problems of spurious reflections from the site building onto the fence were experienced. There were excessively large metallic areas on the building, only portions of which

(a) Side view.

(b) Front view showing serrations.

Fig. 27. Experimental setup.

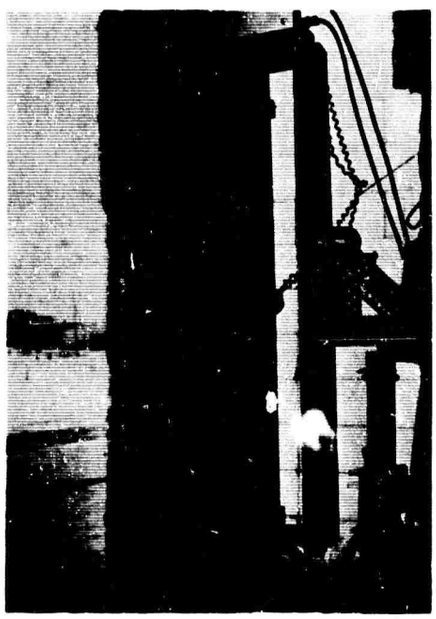

Fig. 28. Probe tower.

could be covered with absorbing material as shown in Fig. 27. (This problem would not exist for the full-size antenna which is taller than the surrounding buildings.) The inner side of the fence was covered with absorbing material to reduce some of the multiple reflections. However, a sufficiently wide strip near the top of the fence was left bare to avoid interfering with the serrations when they were introduced. This bare strip was shown to perturb the diffracted field appreciably at low signal levels. By tilting the fence and increasing the absorber-covered areas on the building, some of this interference was eliminated.

C. Experimental Procedure

The field distribution at the dish aperture was measured with a small horn which was fastened to a movable carriage on the tower shown in Fig. 28. The apparatus was instrumented for automatic operation with a standard antenna pattern recorder. To minimize pickup of spurious signals, absorbing material with a small gap for the waveguide at the neck of the horn was placed in front of the tower.

Clutter suppression of the fence was determined by taking an elevation pattern of the model dish with and without a fence. The difference in signal level gave a measure of the fence effectiveness at all elevation angles for the particular test site and model dish geometry. The pedestal supporting the model dish and the probe tower were mounted on a large turntable, which could be easily turned to place either dish or probe in test position. Nearly all the data were taken with the serrations installed in place. Metallic strips were used to cover the serrations and thus obtain a straight-edge fence; this provided a valuable check and quick evaluation of the edge treatment. The term "covered fence" will be used to indicate absence of edge treatment, while "straight fence" will refer to the linear (as distinguished from the circular) fence. All the experimental data presented in this section of the report are for the straight and vertical fence having the following full-size dimensions:

Distance = 500 ft

Height = 100 ft

Length = 850 ft

D. Straight "Covered" Fence

An early measurement program[12] for the full-scale fence distances of 200, 400 and 800 ft at a number of heights showed reasonable agreement with the theoretical calculations summarized in Fig. 5. Similar results were obtained for vertical and horizontal polarization.

More detailed data were taken for the case corresponding to a 100-ft fence at a distance of 500 ft. The measured vertical field distribution behind the fence is compared with the theoretical curve in Fig. 29. The curve obtained with a large horn shows larger attenuation as it discriminates against off-axis signals; the small horn shows better agreement. There is slight perturbation of the field below the 20-db level caused by multiple reflections at the site, but this did not appear to affect the results significantly.

A measure of the reduction of clutter received by the model dish is presented in Fig. 30. The upper (solid) curve is a conventional elevation pattern taken without the fence. The main beam was taken with 30-db attenuation so it could be displayed on the same chart for calibration purposes. The side lobes are not as narrow, nor do they decay as rapidly as one would expect.

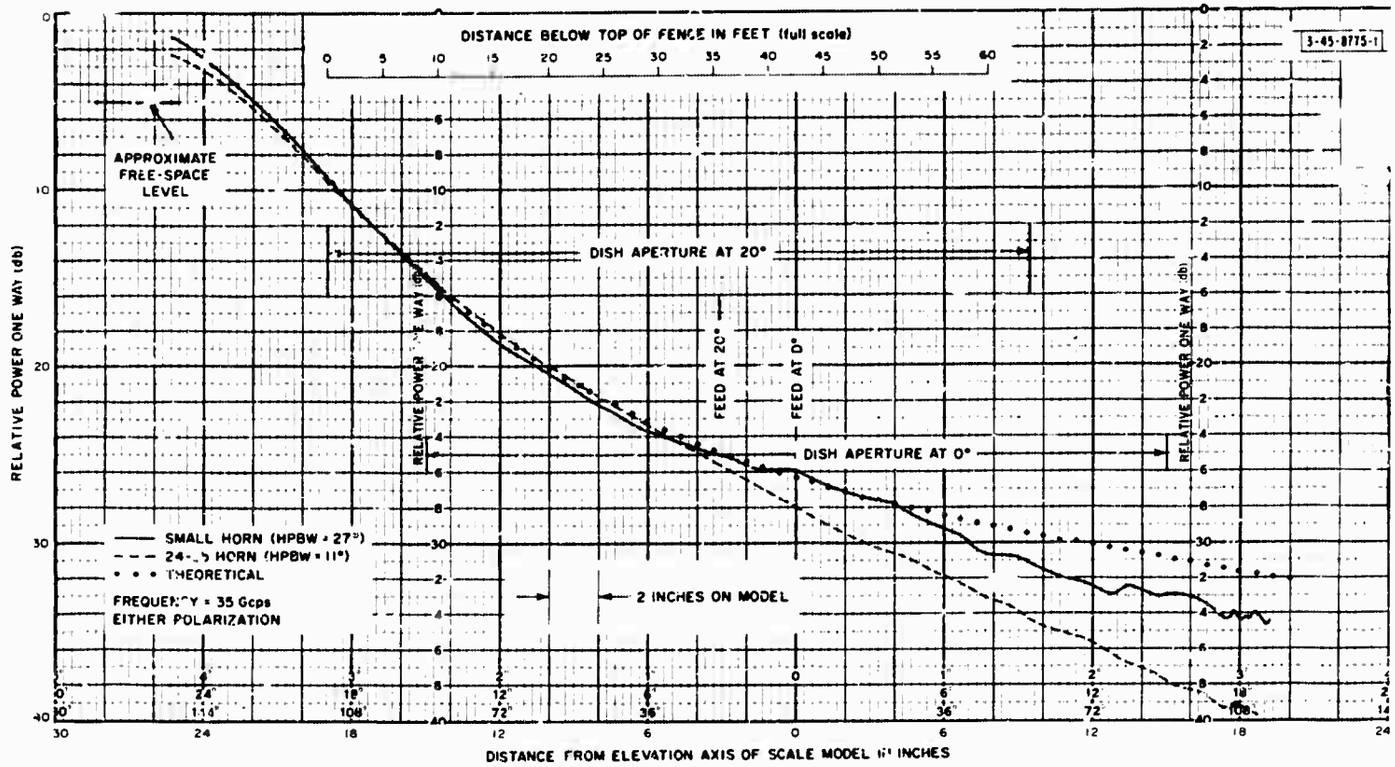

Fig. 29. Measured vertical field distribution at dish aperture for covered (knife-edge) fence.

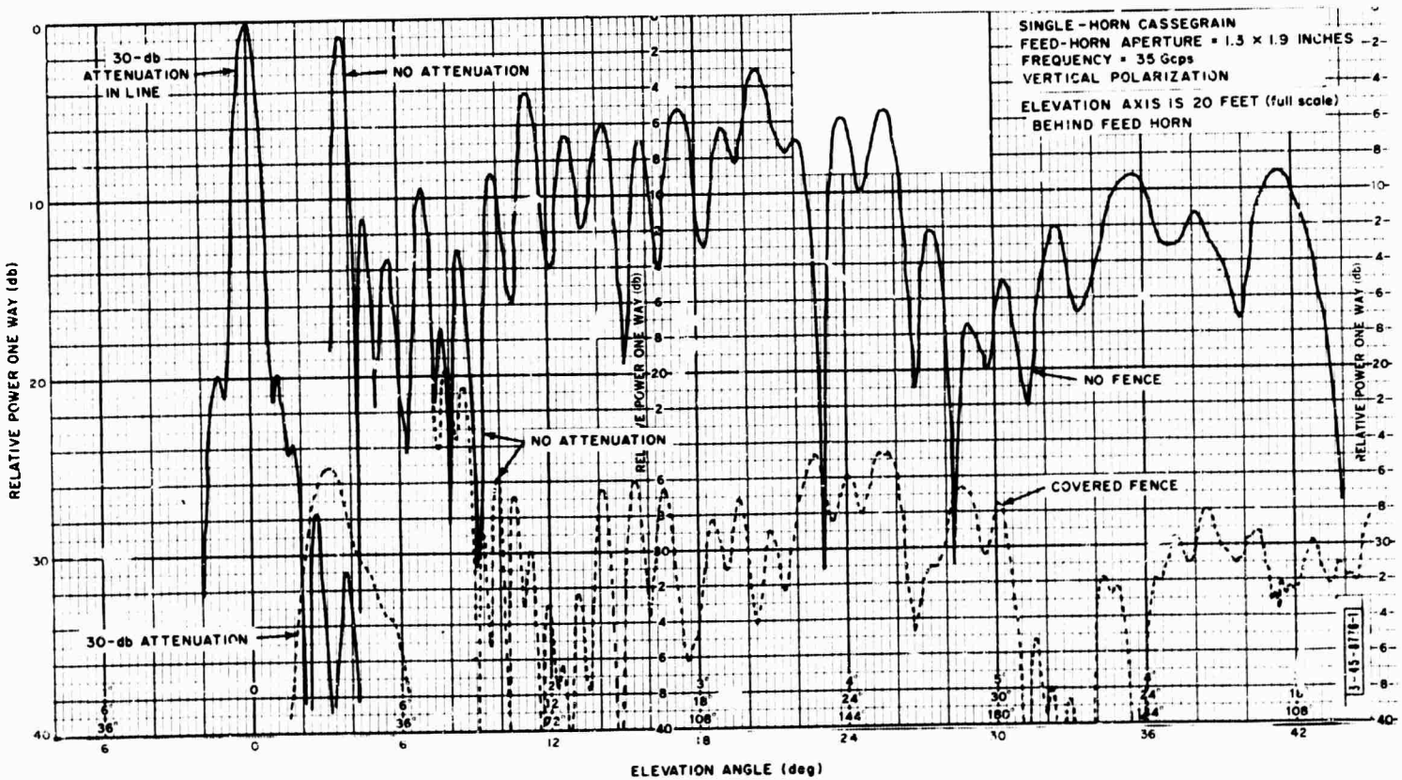

Fig. 30. Measured elevation pattern of model dish with and without covered (knife-edge) fence.

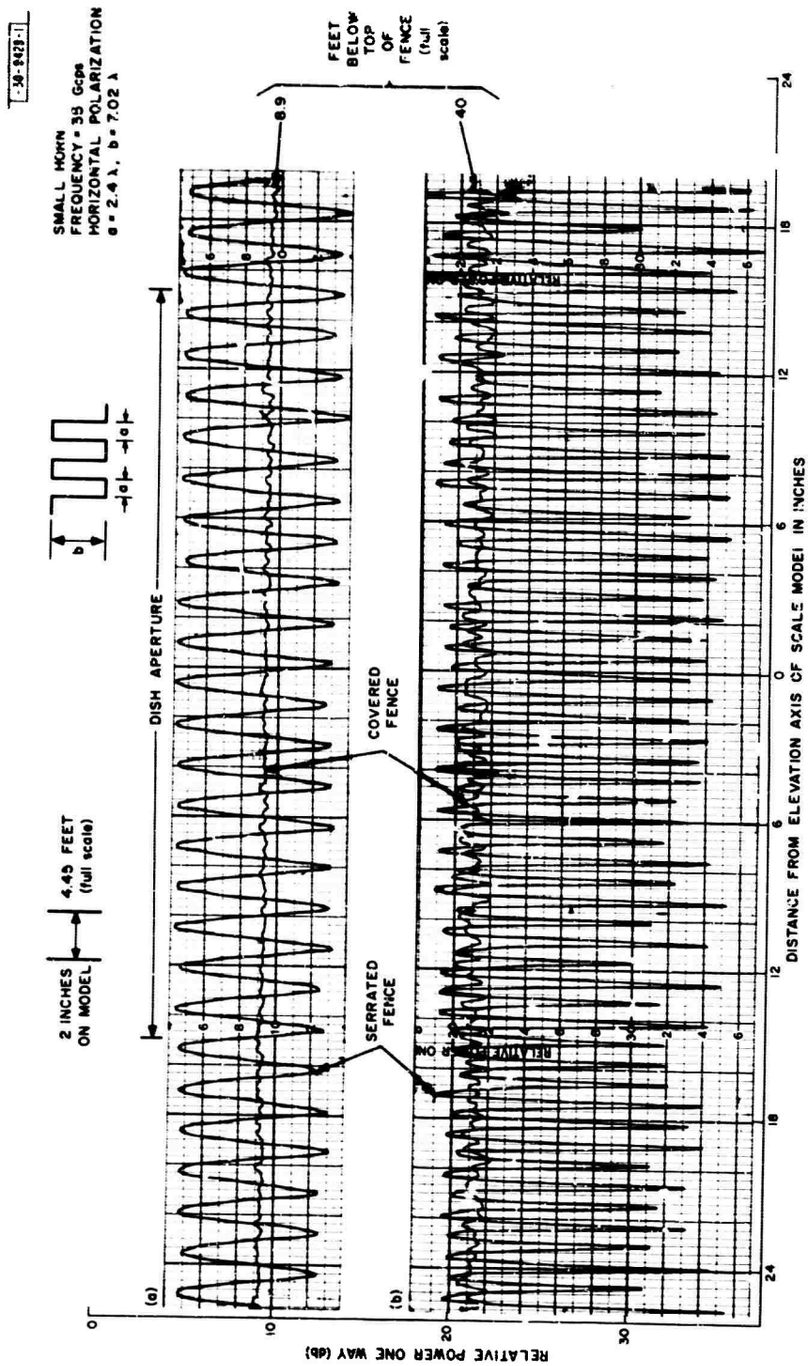

Fig. 31. Measured horizontal field distribution for 2.4λ serrations.

Examination of the primary feed patterns leads to identification of much of this radiation as direct forward spillover past the subreflector. The lower (dashed) curve is an elevation pattern taken in presence of the covered fence. The level of this curve is generally above 20 db below that of the solid curve, which is in good agreement with Fig. 5. Although there is no exact one-to-one correspondence between the two curves, an approximate correspondence is observed if the dashed curve is moved down (to the left) about 3°. This is evidently due to the apparent line source at the top of the fence, which now becomes a clutter source of reduced intensity. Below 7.8°, the dish beam cylinder becomes obscured by the fence; clutter is not suppressed appreciably in this region and is actually increased at some angles. For example, at 3° there is a maximum, corresponding roughly to the dish looking at the line source at the top of the fence.

E. Straight Fence with Wide Serrations

The theoretical analysis in Sec. II-C-4 showed that wide serrations are subject to "resonances." This was confirmed in some detail for the case of simple serrations. Figure 31 presents typical small-horn probes of the field in the horizontal plane for 2.4λ serrations. The data were taken at two different heights in the aperture region of the model dish. The predicted doubling of the spatial "frequency" in the cancellation region is evident in part (b) of the figure. By using the large horn, we obtained generally similar results, except that in the cancellation region the peak level of the oscillations was about 3.5 db below the level of the covered fence. When allowance was made for the directivity of both horns at the angle (12°) corresponding to the first resonant region, the true peak of the oscillations was estimated to be about 3.5 and 5.5 db above the level of the covered fence for the small and large horn, respectively. The theoretical value is nearly 8 db [see Eq. (22)].

Below the cancellation region, the peak of the oscillations tended to rise again with respect to the level of the covered fence, and the spatial frequency tended to return to that near the top of the aperture, in accordance with theory.

A polarization sensitivity was observed, since the apparent cancellation region occurred about 4.5 ft (full scale) higher for vertical polarization than it did for horizontal polarization. This region could be identified by the doubling of spatial frequency and the observation of minimum peak signal with respect to the covered fence level. Deep nulls between peaks usually occurred in this region. Consideration of inductive and capacitive gratings will show that the phase shift of each is of the proper sign to displace the cancellation region in the observed direction.

Clutter suppression with the 2.4λ serration was found to be neither uniform nor substantially improved when the elevation pattern of the model dish was compared with that for the covered fence.

When the serration width was reduced to one wavelength, the fence behaved in a similar way. The measured level of the oscillations in the cancellation region was lower, as seen in Fig. 32. However, this was due to the directivity of the small probe horn at 30° off axis, where the first resonance occurs for $a = \lambda$. After allowance was made for this, the peak level of the oscillations was estimated to be a few decibels higher than the predicted figure of 7.5 db above the level of the covered fence.

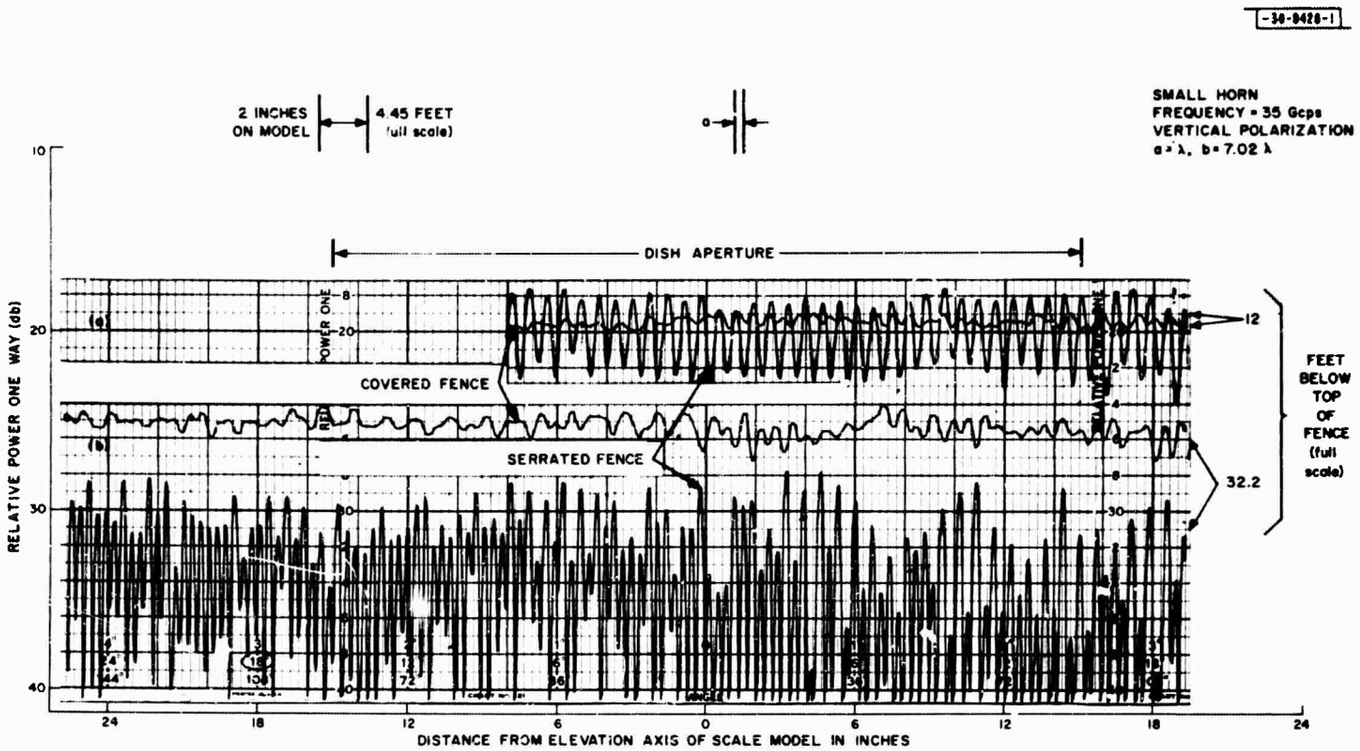

Fig. 32. Measured horizontal field distribution for 1λ serrations.

F. Straight Fence with Narrow Serrations

Since the theory appeared to be supported by the experimental results, a sufficiently narrow serration was chosen, so there was no predicted resonance on the experimental fence. It was expected that polarization sensitivity would increase for the narrower slots, and this is clearly shown in Fig. 33 for a = 0.65λ. The centers of the cancellation region have a deep null in the case of both polarizations, and they are now separated by about 13 ft (full scale). There was a fluctuation in this separation amounting to several feet over the course of an extended measurement period. For 45° polarization, the null occurred midway between those shown in the figure.

Figure 34 shows the virtual elimination of the horizontal plane oscillations, as predicted for this serration width. A substantial reduction in the residual signal was achieved when the same fence was temporarily inclined about 14° away from the vertical. This is evidently a further manifestation of low-level multiple reflections at the site which could not be eliminated without an excessive amount of effort. The actual field at the cancellation level may consequently be considerably below that shown in Fig. 34.

A measure of the clutter suppression in the case of vertical polarization is given in Fig. 35 for a suitable null location. The additional clutter reduction of the serrated fence is seen to be somewhat uneven, averaging about 8 db for a dish elevation angle greater than 20°. When the null location was varied by changing the serration length b, the results showed that its position was not critical when the feed horn offset from the elevation axis was 20 ft (full scale). Maximum suppression occurs when the feed horn is in the null, as will be shown in Sec. III-G.

The null position in the case of horizontal polarization was much too low when vertical polarization was optimized. However, clutter suppression tended to be quite similar for either polarization for the same null height.

Some methods for equalizing the null locations were tried. A strip of metal up to about $\frac{2}{3}\lambda$ wide raised the location of the nulls of both polarizations a distance of about 5 ft (full scale) when placed across the top of the serrations. Greater width tended to make the null narrower and shallower. When this strip was replaced by closely spaced horizontal wires, the null of the horizontal polarization was selectively raised. Additional selective raising of the horizontal polarization null was achieved by stretching wires horizontally across the serrations and separating them by a distance comparable to the serration width a (Fig. 36). Good contact was necessary. The diameter of the wires was about 0.6 in. (full scale), but this is probably not critical. It is possible that both approaches may bring the nulls sufficiently close together, although this was not explored in detail because of difficulties of implementing these procedures accurately on the existing scale model.

Further experimental work is required to determine the effect of the thickness of the experimental serrations. For mechanical rigidity at the scale-model size, these were cut into a metal sheet 0.18λ thick. No doubt this increased the observed polarization sensitivity. A possible approach is to use printed-circuit techniques to construct very thin serrations for model work. It was found that a fiberglass sheet about λ/30 thick did not disturb the null when placed over the 0.65λ serrations, if it extended sufficiently far above the top of the fence. Substantially thicker sheets gave trouble in the cancellation region. Apparently, this technique may be used if care is taken to avoid such problems.

The frequency response of the thick experimental serrations also raised some problems. No detailed measurements were made but the available data for vertical polarization show that,

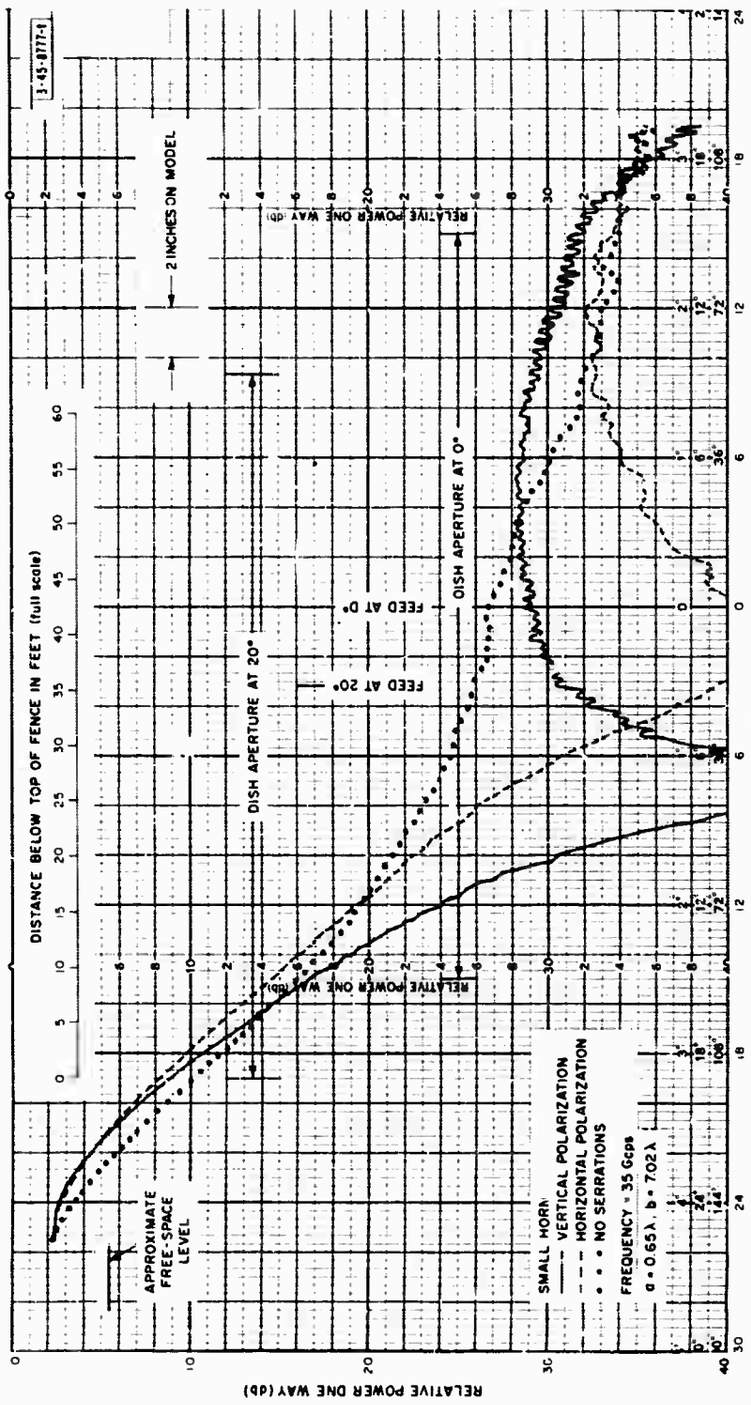

Fig. 33. Measured vertical field distribution at dish aperture of 0.65λ serrations.

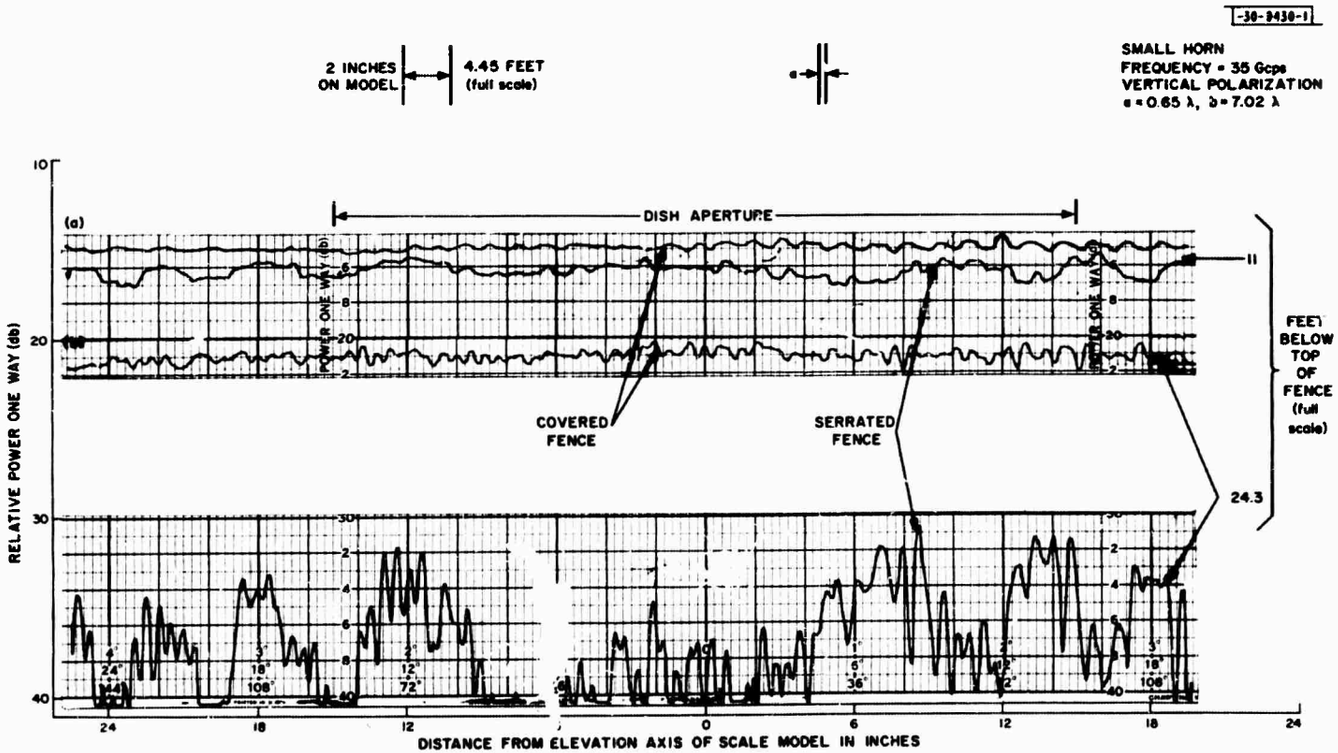

Fig. 34. Measured horizontal field distribution for 0.65λ serrations.

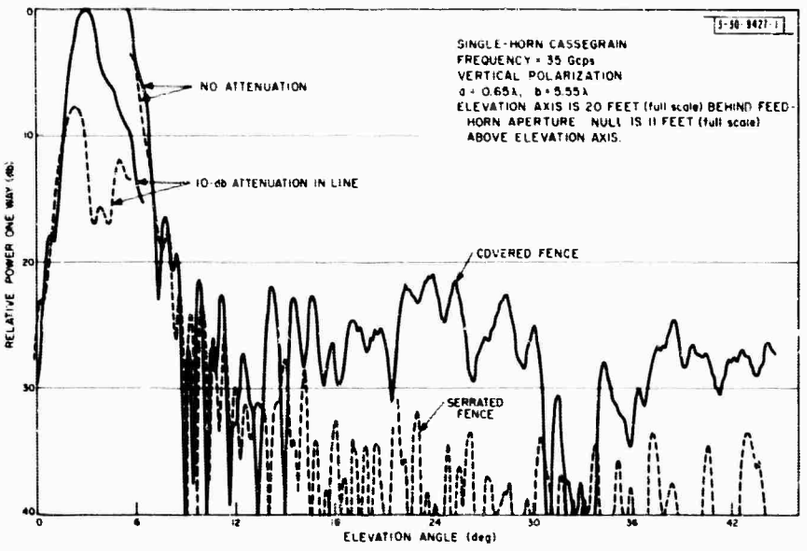

Fig. 35. Measured pattern of model dish in presence af covered (knife-edge) and serrated fence.

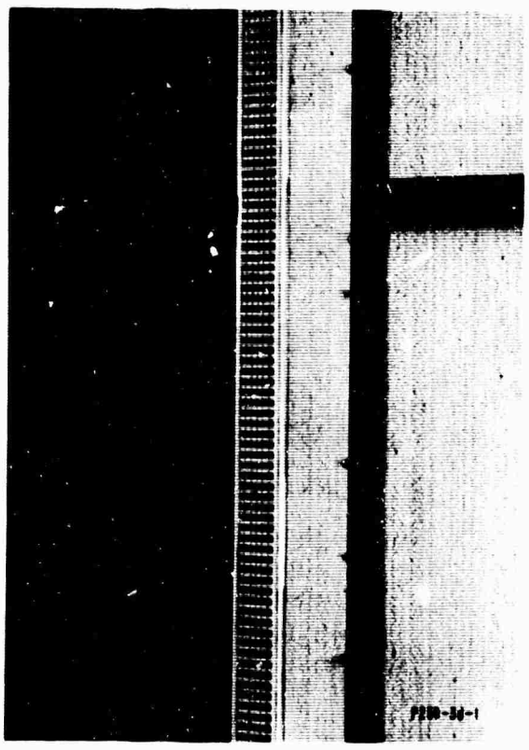

Fig. 36. Method for equalizing null location.

as λ increased, the null moved up, contrary to expectations. At $a/\lambda = 0.5$, the null moved up a distance of about 6 ft (full scale) and became quite shallow. For horizontal polarization, the null moved down as expected. Since it occurred at a fairly low signal level for the particular serrations under test, the effect on null depth is uncertain, although its motion appeared even more pronounced than for vertical polarization.

Some efforts were made to increase the width of the cancellation region and thus increase clutter suppression over a greater range of elevation angles. The possibility of staggering serration depth, while keeping their tops at the same height, was explored. This was easily done on the model fence with aluminum tape on the bottom of every other slot. Various combinations led to the conclusion that some broadening is possible but at the expense of creating horizontal plane oscillations in the cancellation region. This is a fairly complicated effect directly related to the increase in effective a due to the staggered serration depth. The technique did not appear promising.

To double-check the theory, the fence distance was reduced to 214 ft (full scale). This increased the angle intercepted by the fence at the probe horn well beyond the point where the first resonance condition was satisfied. The particular portions of the serrated edge generating the "grating lobes" were then identified by successively covering sections of the fence. The theory was again vindicated. Moreover, it was found that relatively small portions of the entire fence length were in resonance for a fixed observation point. The effect of the resonance, as seen previously for the wider serrations, was to introduce oscillations of period 2a in the horizontal plane. The period of the oscillations was reduced to a in the cancellation region only when the resonant sections on either side of the observation point were uncovered simultaneously. When allowance was made for the directivity of the probe horn, the peak of the oscillations was estimated to be much above the level of the covered fence.

G. Optimum Geometry for Clutter Reduction

Since it was recognized that a great deal of the clutter was caused by feed spillover, it was of interest to determine the maximum benefit possible with a resonance-free serrated fence. Therefore, the model dish was temporarily remounted on the test pedestal so that the elevation axis of rotation passed through the feed-horn aperture. This kept the horn at the same point for all elevation angles. Serration length b was next adjusted to place the null at the center of the horn. The result of this measurement, as limited by available transmitter power and by residual site fields, is shown in Fig. 37. Clutter reduction is substantially greater than in the case of the offset dish, as shown in Fig. 35. Again, similar results were obtained for both polarizations for identical null positions. When the null position was raised, or lowered, the clutter suppression decreased.

H. Round Serrated Fence

The chord approximation of the round fence was trouble free when its edge was covered. The serrated edge introduced the expected resonance as well as some other difficulties. At first, the four fence sections were placed upright along chords of the circle corresponding to a radius of 500 ft. A horizontal probe of the field in the cancellation region showed a relatively high residual signal level with superimposed oscillations. However, the peak value of these oscillations was still well under the covered fence level. By covering successive sections of

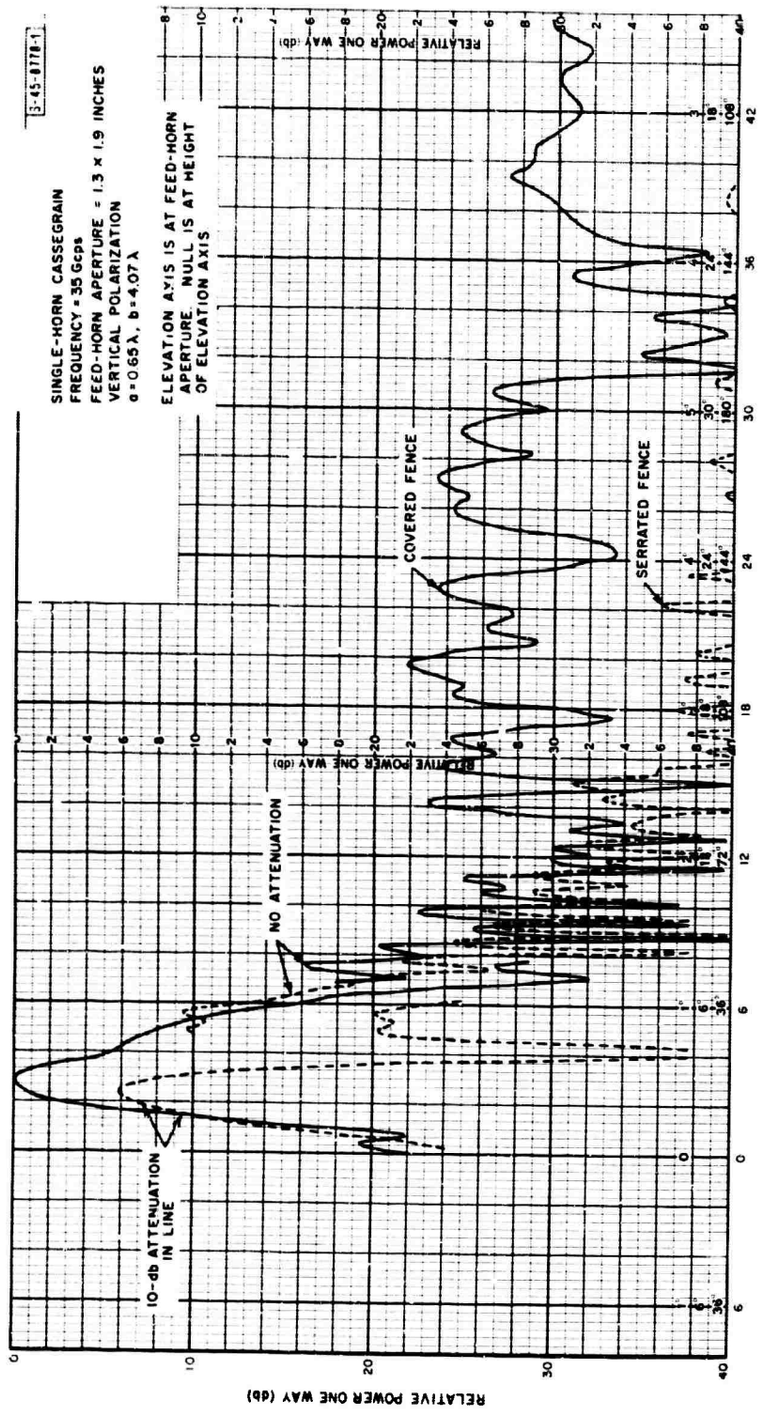

Fig. 37. Measured elevation pattern of model dish in presence of covered (knife-edge) and serroted fence.

the serrations, it was demonstrated that appreciable signal strength was originating near the far ends of the fence. Examination of the chord geometry and reference to Figs. 16, 19 and Sec. II-C-6 will show that the "grating lobes" for a = 0.65λ are directed radially inward (Θ = 0) at an angle somewhat smaller than that intercepted by the far end of the fence. At other points on the fence, "grating lobes' will also exist, but they will not be directed radially inward, i.e., $|\Theta| > 0$. Similar results were obtained for both polarizations.

The chord fence was next inclined about 15° away from the probe in an attempt to reduce the high residual field in the cancellation region. Polarization sensitivity to inclination was immediately noted. For vertical polarization, the cancellation region appeared fairly clean with a good deep null. However, the situation for horizontal polarization was quite complicated. The cancellation region was very irregular, and its height varied excessively as the field was probed in the horizontal plane. At this polarization, null position was found to be quite sensitive to changes in the shape of the fence, there being a large shift downward. The trouble seemed to originate in the vertex area of the chords. When a straight inclined fence was deformed slightly to check this problem, similar behavior occurred only for horizontal polarization.

Since the existing scale model was not amenable to further changes in fence shape, no investigation was made of smaller chords or a perfectly circular geometry. Although tolerance problems were troublesome at the scale-model size, the good performance for vertical polarization would seem to rule this out as an explanation of the poor performance of the inclined chord fence at horizontal polarization.

I. Further Edge-Treatment Considerations

Both theory and experiment bring out the basic limitation of any periodic structure similar to the serrations. Under restricted conditions, narrow serrations can be very useful (as shown in Figs. 35 and 37). When a long, or round, fence is necessary, the presence of resonances can be avoided with nonperiodic edge-treatment techniques. One possible alternative is given in Fig. 38. The basic idea is to place a line source of the proper amplitude at the appropriate distance below the top of the fence, so it will interfere with the apparent line source at the top

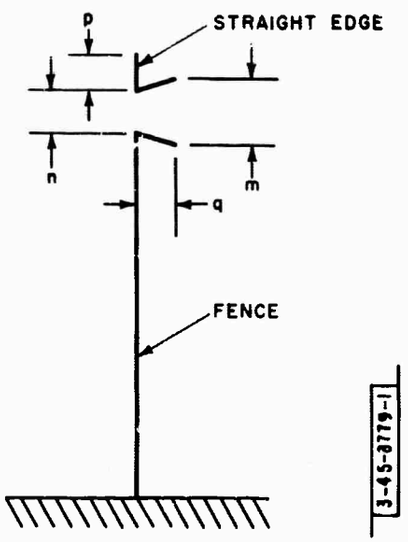

Fig. 38. An alternative approach to edge treatment.

of the fence and cancel at the desired point in the aperture. A rather crude experiment showed that a simple gap some distance below the top of the fence gave inadequate cancellation. By adjusting the collecting aperture m to several wavelengths and the radiating aperture n to about one wavelength, deep nulls were obtained which were nearly coincident for vertical and horizontal polarization. The length q provides phase control, and p provides some control over null width. A combination of two or more such line sources is conceivable. Although the upper structure requires supports and appears more troublesome mechanically than the simple serrations, its implementation may be straightforward once the parameters are determined experimentally.

IV. CONCLUSIONS

Scale-model measurements verified the theoretically predicted field distribution behind a straight edge.

The effectiveness of edge serrations in creating a null or cancellation region behind the fence as also experimentally verified. However, the width of the serrations had to be sufficiently small to prevent the appearance of grating lobes or resonant regions along the length of the fence. The existence of these grating lobes generally negated any increase in clutter suppression provided by the serrations. An adequate theory was developed to explain these resonant effects. The narrow serrations also yielded a null or cancellation region whose position was polarization sensitive.

Because of the resonant effect and the polarization sensitivity, it was concluded that for long fences continuous horizontal slots or other nonperiodic structures should be investigated.

For the particular geometry of the AMRAD radar, it would be prohibitively expensive to produce a one-way clutter suppression in excess of about 22 db without serrations. For various economic and tactical reasons, a roughly triangular fence 100 ft high and at a distance of 500 ft in the tracking sector was chosen. This fence has a nominal one-way clutter suppression of 20 db. At an elevation angle of 7.8°, the antenna beam cylinder just grazes the top of the shield and operation of the radar is affected. However, satisfactory elevation tracking is possible down to about 4°, although at reduced range sensitivity. For this elevation, the two-way gain reduction is about 12 db.

The response of the large AMRAD antenna to the complex fence-diffracted field was determined by measurement on a scaled AMRAD antenna. The expected 20-db one-way clutter suppression was verified.

We found that properly designed serrations could produce an additional 10-db one-way clutter suppression. However, because of the polarization sensitivity mentioned and the vertical movement of the center of the actual AMRAD antenna, perhaps only a 5-db additional average clutter suppression will be practically realized.

Extensive on-site clutter measurements and correlation with the terrain topography indicated that a 20-db one-way suppression would be adequate for this installation. The edge serrations were therefore not incorporated in the present shield.

Should the radar performance be upgraded so that additional clutter suppression is required, the narrow serrations may be installed. An additional 5 db, on the average, can be obtained by installing serrations 9 in. wide and 5.3 ft tall along the top edge.

ACKNOWLEDGMENTS

The authors wish to thank Dr. W. W. Ward for his support and encouragement. Dr. K. J. Keeping and J. G. Jelatis provided advice at the early stages of the investigation; E. F. Pelrine assisted in the experimental measurements. The cooperation of L. Niro and his staff at the Lincoln Antenna Test Facility is appreciated.

REFERENCES

1. W. G. Carlson and W. W. Cannan, "The High Fences at White Sands," Electronics 36, 64 (18 October 1963).
2. F. K. Preikschat, "Screening Fences for Ground Reflection Reduction," Microwave J. 7, 46 (August 1964).
3. J. Ruze, "Preliminary Investigation of Clutter Fence for AMRAD Radar" (10 October 1963); "Additional Clutter Fence Calculations for AMRAD" (22 October 1963); "Shielding Fence Calculations (AMRAD)" (13 November 1963); "Redesign of AMRAD Feed (Estimate of Side Lobe Level from Various Causes)" (31 January 1964). Lincoln Laboratory Internal Memoranda (not generally available).
4. J. E. Becker, "Design Study for AMRAD Anti-Clutter Fence," Report No. 1233, Wheeler Laboratories, Inc., Smithtown, N.Y. (22 July 1964).
5. M. Born and E. Wolf, Principles of Optics, Secs. 8.7 and 11.5 (Pergamon Press, New York, 1959).
6. "TABLISTY Integralov Frenela," USSR Academy of Science, Moscow, 1953.
7. W. Gautschi, "Error Function and Fresnel Integrals," in Handbook of Mathematical Functions, Natl. Bur. Standards AMS-55 (1964), pp. 300-302.
8. M. J. Ehrlich and W. G. Stems, "A Method for the Reduction of Edge Diffraction Effects," Symposium on Microwave Optics, McGill University, Montreal, June 1953.
9. M. Takado and M. Shinji, "An Application of the Diffractor Grating to the 11 Gc/s. Microwave Systems," Trans. G-AP 13, No. 4, 532 (July 1965).
10. T. Hasegawa, et al., "MM-Wave Model Experiments of Diffraction Field by Knife Edges," International Conference on Microwaves, Circuit Theory and Information Theory, Tokyo, 1964, pp. 311-312.
11. W. Cohen and C. M. Steinmetz, "Amplitude- and Phase-Sensing Monopulse System Parameters, Part II," Microwave J. 2, 33 (November 1959).
12. F. I. Sheftman, "Experimental Investigation of AMRAD Fence at 1/24 Scale" (12 March 1964), Lincoln Laboratory Internal Memorandum (not generally available).

DOCUMENT CONTROL DATA – R&D

(Security classification of title, body of abstract and indexing annotation must be entered when the overall report is classified)

1. ORIGINATING ACTIVITY *(Corporate author)*
Lincoln Laboratory, M. I. T.

2a. REPORT SECURITY CLASSIFICATION
Unclassified

2b. GROUP
None

3. REPORT TITLE
Radar Ground-Clutter Shields

4. DESCRIPTIVE NOTES *(Type of report and inclusive dates)*
Technical Report

5. AUTHOR(S) *(Last name, first name, initial)*
Ruze, John Sheftman, Franklin I. Cahlander, David A.

6. REPORT DATE	7a. TOTAL NO. OF PAGES	7b. NO. OF REFS
19 August 1965	48	12

8a. CONTRACT OR GRANT NO.	9a. ORIGINATOR'S REPORT NUMBER(S)
AF 19(628)-5167	Technical Report 399
b. PROJECT NO. ARPA Order 498	9b. OTHER REPORT NO(S) *(Any other numbers that may be assigned this report)*
c.	ESD-TDR-65-325
d.	

10. AVAILABILITY/LIMITATION NOTICES
Distribution of this document is unlimited.

11. SUPPLEMENTARY NOTES	12. SPONSORING MILITARY ACTIVITY
None	Advanced Research Projects Agency, Department of Defense

13. ABSTRACT

Metal shields (or fences) are useful in reducing the ground clutter received by a radar. The design of a clutter shield for an L-band radar employing a 60-ft parabolic reflector with Cassegrainian geometry is verified by scale-model measurements at K_a-band. It is shown that a 100-ft fence, at a distance 560 ft from the radar, will give a nominal one-way clutter reduction of 20 db. Tracking is expected to be virtually unaffected down to about 7.8° in elevation, but the low limit on useful performance is about 4.8°. More than 10-db additional clutter reduction is achieved by cutting rectangular slots in the top edge of the fence. However, these and other periodic structures are subject to "resonances" related to grating lobes. This phenomenon is investigated experimentally on the scale model and explained by a mathematical analysis utilizing the principle of stationary phase. A proposed nonperiodic edge treatment is expected to be free of this troublesome effect.

14. KEY WORDS

ground-clutter shields
radar fences
Cassegrainian geometry
diffraction, knife edge
diffraction, edge serrations
Fresnel integrals
stationary phase